PETROLOGY OF THE ALH-77003 CHONDRITE (C3)

Yukio IKEDA

Department of Earth Sciences, Ibaraki University, Bunkyo 2-chome, Mito 310

Abstract: The ALH-77003 chondrite (C3) is made up of fine-grained CAI's, amoeboid olivine inclusions, chondrules, devitrified glass fragments, mineral fragments and matrix. Their bulk chemical compositions and the constituent mineral compositions are presented in detail, and their origins are discussed. The fine-grained CAI's were formed from the materials rich in fassaitic pyroxenes by reactions with the surrounding gas at low temperatures. Amoeboid olivine inclusions are considered to have a cogenetic relationship with fine-grained CAI's and to have suffered the same reactions as the fine-grained CAI's. FeO-rich chondrules (fSP type), devitrified glass fragments and matrix were formed from the solar nebula condensates at low temperatures whereas MgO-rich chondrules (mIP and mSP) types were formed from high temperature condensates.

1. Introduction

The ALH-77003 chondrite is classified as a C3 chondrite (Antarctic Meteorite Newsletter, **4**(2), 1981). Fine-grained Ca- and Al-rich inclusions (CAI's hereafter) and amoeboid olivine inclusions (AOI's) are abundantly present in the chondrite, supporting this assignment, and the abundant occurrence of chondrules in this chondrite means that it is not a CI nor CM type. The bulk chemical composition of this chondrite (MARVIN and MASON, 1980) gives the following atomic ratios: Al/Si, 0.10; Mg/Si, 1.03; Ca/Si, 0.070; and Fe/Si, 0.772. According to Wasson's criteria (WASSON, 1974) for classification of CV and CO types, these ratios of Al/Si and Ca/Si with the high ratio of chondrules/matrix of this chondrite show it to be a CO type, whereas the Fe/Mg ratio of 0.752 means the chondrite is a CV type. The atomic ratios of Al/Mn and Ca/Mn of this chondrite are 13 and 9.1, which are rather near the CM type and far from the values of CO and CV (KALLEMEYN and WASSON, 1981). Chondrule sizes are also a criterion for distinguishing between CV and CO (WASSON, 1974), but are not used for grouping this chondrite because they range widely from 0.08 mm up to 1.2 mm in diameter. MCSWEEN (1977c) showed that excentro-radial pyroxene chondrules are not observed in CV type, which includes melilite-anorthite chondrules instead. From this point, ALH-77003 can be classified as CO because of the occurrence of devitrified glass chondrules equivalent in chemical composition to excentro-radial pyroxene chondrules, and because it lacks melilite-anorthite chondrules. According to VAN SCHMUS and HAYES (1974), one criterion for the subdivision of CV and CO is the amount of opaque minerals in chondrules. However, this is not effective for this chondrite because some chondrules include opaque minerals abundantly whereas some do not. Hence, ALH-77003 can not be classified into CI, CM, CV and CO

types, and may be considered an unique C3 chondrite.

In general, C3 chondrites consist of CAI's, AOI's, dark inclusions, chondrules, mineral fragments, matrix and so on. The CAI's have been well studied and are classified into two categories according to grain sizes of the constituents, coarse-grained CAI's and fine-grained CAI's. The former and the latter together with AOI's are further classified into several types, respectivery (MARTIN and MASON, 1974; GROSSMAN, 1975; WARK and LOVERING, 1978; WARK, 1979; KORNACKI, 1981; ARMSTRONG *et al.*, 1981). Petrological and petrochemical studies on the other constituent units, chondrules, dark inclusions or lithic fragments, mineral fragments, and matrix also have been performed (OSBORN *et al.*, 1974; GREEN *et al.*, 1971; MCSWEEN, 1977a, b, c, d; MCSWEEN and RICHARDSON, 1977; WARK, 1978; BUNCH and CHANG, 1980). However most of these studies are concentrated on a few C3 chondrites, especially on Allende meteorite.

In this paper, the petrological and petrochemical study of the constituents of ALH-77003, fine-grained CAI's, AOI's, chondrules, devitrified glass fragments and matrix are presented, and the genetical relationships among them are discussed.

2. Petrography

ALH-77003 is a massive aggregate of fine to medium-grained CAI's, AOI's, chondrules, devitrified glass fragments, silicate and opaque mineral fragments and matrix. Fine-grained CAI's occur as irregular-shaped black to gray aggregates smaller than 0.5 mm, consisting of fine-grained materials usually finer than micron size, but in some medium-grained CAI's relatively large spinel grains up to several tens microns and/or fassaitic pyroxene grains not so large as spinel graines are rarely observed. These fine to medium-grained CAI's often have a thin rim, usually micron size in width, of aluminous high-Ca pyroxenes. They are usually free from opaque minerals. A botryoidal olivine inclusion (Fig. 7f) is present. It consists of nodules, several tens up to one hundred microns in diameter, and interstitial materials, the former being rich in spinel and the latter consisting mainly of fine-grained olivine. Textual variety similar to the botryoidal olivine inclusion is observed in some fine to medium-grained CAI's and AOI's, showing continuous spectrum between them. AOI's are irregular-shaped aggregates smaller than about 0.5 mm across, consisting mainly of olivine graines of several to several tens micron size. AOI's sometimes include small amounts of irregular-shaped patches consisting of very fine-grained materials, and commonly comprise variable amounts of opaque minerals such as Fe-Ni metals and troilite.

The chondrules, which are considered to have crystallized from molten droplets, occur abundantly and show clear outlines against the matrix. A variety of textures exists, the commonest being porphyritic to granular olivine chondrules. Barred olivine chondrules and porphyritic pyroxene chondrules are also observed in minor amounts. Typical radial pyroxene chondrules are not observed, but fine-grained pyroxene or devitrified glass chondrules which are equivalent to the radial pyroxene chondrules in chemical composition sometimes occur. A rare type of porphyritic diopside chondrules occurs, consisting of nearly pure diopside crystals set in clean glass

(Fig. 7a).

Silicate mineral fragments are mainly olivine or low-Ca pyroxene which show often compositional zoning with ferrous rims. Opaque mineral fragments are kamacite, taenite, troilite and mixtures of them. Kamacite occurs more commonly than taenite.

Devitrified or brown glass fragments show angular to subround outlines, about several hundred microns across. They may be fragments of larger glasses or larger glassy chondrules.

The matrix is defined as aggregates of materials finer than micron size filling interstitial spaces between the inclusions, chondrules and mineral fragments.

3. Chemical Compositions of Inclusions, Chondrules, Devitrified Glass Fragments and Matrix

The chemical compositions of fine to medium-grained CAI's, AOI's, chondrules, devitrified glass fragments and matrix were obtained using a defocussed beam of an electron-probe microanalyzer. The correction method of the analytical data is

Table 1. Chemical compositions of fine to medium-grained CAI's. Two inclusions, Nos. 71–1 and 105, are intermediate type between fine-grained CAI and AOI.

	31	34	44′	51–3	51–4	51–7	69	71–1	74	87	103	104
Na_2O	8.95	9.17	0.16	4.30	8.11	2.89	3.89	5.39	7.75	7.95	5.76	5.44
MgO	5.62	3.50	11.16	8.61	8.03	5.95	10.82	13.19	3.75	5.74	9.25	8.51
Al_2O_3	32.50	37.53	47.98	30.31	23.88	43.94	19.38	15.16	35.01	42.36	21.05	32.61
SiO_2	29.27	25.91	12.95	30.85	37.46	20.80	40.81	45.26	30.85	21.48	42.23	30.66
K_2O	1.22	1.43	0.00	0.38	0.01	0.73	0.16	0.08	1.33	1.18	0.18	0.19
CaO	5.67	4.01	6.99	10.94	10.39	10.23	15.69	8.52	6.18	2.73	15.82	9.67
TiO_2	1.39	2.16	2.23	0.62	1.05	0.90	1.11	0.18	1.02	0.92	0.61	0.91
Cr_2O_3		0.09								0.10	0.09	0.55
MnO			0.33					0.19	0.00			
FeO	9.66	8.80	15.79	7.53	4.64	8.90	2.95	9.30	6.51	12.99	2.18	8.03
Total	94.27	92.59	97.29	93.55	93.59	94.34	94.81	97.27	92.40	95.46	97.16	96.56

	105	336–1	343	347–2	361–1	361–2	377	382	384	389	394–1
Na_2O	3.93	6.77	5.73	4.63	8.29	8.34	8.72	2.85	6.28	2.96	3.88
MgO	15.01	7.33	10.23	9.71	4.01	6.62	8.87	8.67	6.85	9.03	11.05
Al_2O_3	14.86	37.49	21.37	26.72	33.56	31.27	20.45	41.85	48.65	32.10	26.60
SiO_2	36.26	27.73	37.42	31.05	25.43	28.29	47.25	19.60	18.75	27.20	33.62
K_2O	0.15	1.17	0.43	0.80	1.44	1.10	0.51	0.41	1.00	0.42	0.54
CaO	7.26	6.60	9.97	8.72	5.51	3.59	11.77	8.46	4.11	13.04	12.65
TiO_2	0.57	1.58	0.41	1.40	1.55	0.99	0.88	1.80	1.16	4.06	1.22
Cr_2O_3	0.27										
MnO											
FeO	17.17	9.39	9.29	9.48	14.53	14.67	2.92	13.19	10.61	10.32	8.39
Total	95.47	98.05	94.87	92.50	94.33	94.87	101.37	96.82	97.41	99.13	97.95

according to BENCE and ALBEE (1968), and further correction for AOI's and chondrules is performed by the method of IKEDA (1980), because of the heterogeneous occurrence of coarse-grained polyphases in them. Opaque minerals in inclusions and chondrules were avoided from the beam of electron-probe microanalyzer. Thus, the chemical compositions presented here are those of silicates and oxides in inclusions and chondrules. The chemical compositions of them are tabulated in Tables 1 to 6.

3.1. The fine to medium-grained CAI's show a wide variation of chemical composition (Table 1): Al_2O_3, 19–49 wt%; SiO_2, 12–48%; CaO, 2–16%; MgO, 3–12%; FeO, 2–16%; Na_2O, 0.1–10%; K_2O, 0.00–1.5%; and TiO_2, 0.4–4.1%. Their compositions are represented mainly by various mixtures of spinel and high-Ca pyroxene. The chemical compositions of nodules and interstitial materials of a botryoidal olivine inclusion are tabulated in Table 2, the former being rich in spinel component and the latter being rich in normative olivine and high-Ca pyroxene components. The botryoidal olivine inclusion is characteristically poor in alkali contents.

3.2. The chemical compositions of AOI's are: SiO_2, 33–41 wt%; MgO, 20–38%; FeO, 15–34%; Al_2O_3, 1–8%; CaO, 1–6%; Na_2O, 0.01–3.3%; K_2O, 0.00–0.06%; and

Table 2. Chemical compositions of AOI's together with those of nodules (68–2 and 68–4) and interstitial material (68–3) of a botryoidal olivine inclusion.

	39	42′	43	56	59	71–2	84	90	92	95	101
Na_2O	3.23	0.81	0.04	0.49	0.11	2.26	0.82	0.10	0.07	0.56	0.42
MgO	20.64	23.13	28.82	28.92	24.91	24.00	26.89	25.44	28.40	27.66	29.04
Al_2O_3	8.10	6.07	2.74	1.90	2.88	7.77	4.03	1.46	3.70	4.49	6.43
SiO_2	36.96	37.13	35.09	36.69	34.93	40.68	36.06	33.53	37.49	35.65	38.30
K_2O	0.06	0.02	0.00	0.00	0.00	0.00	0.01	0.00	0.00	0.00	0.00
CaO	3.36	3.35	1.89	1.41	2.57	3.96	2.13	1.07	3.45	1.74	5.45
TiO_2		0.22	0.00	0.18	0.00	0.17	0.18	0.00	0.18	0.00	0.36
Cr_2O_3							0.32	0.32	0.31	0.35	0.25
MnO	0.26	0.20				0.17					
FeO	23.21	28.65	31.09	30.84	30.59	22.91	28.14	33.91	24.49	28.75	18.69
Total	95.82	99.58	99.67	100.43	96.00	101.92	98.58	95.83	98.09	99.20	98.94

	110	111	304	329	385	394–2	68–2	68–4	68–3
Na_2O	0.06	0.46	0.47	0.01	0.02	0.44	0.09	0.10	0.02
MgO	30.02	27.33	30.42	33.55	37.55	24.01	12.99	14.37	28.19
Al_2O_3	3.21	4.42	4.37	1.58	3.21	4.28	43.98	51.08	6.63
SiO_2	36.55	37.07	36.38	37.52	36.97	35.34	13.38	9.46	38.65
K_2O	0.00	0.00	0.02	0.01	0.00	0.01	0.00	0.00	0.00
CaO	2.55	3.72	2.25	1.69	2.03	5.21	7.65	7.32	7.95
TiO_2	0.07	0.21	0.28	0.33	0.18	0.20	1.95	4.25	1.01
Cr_2O_3	0.41	0.38							
MnO									
FeO	24.20	25.49	24.26	22.15	14.93	26.39	13.57	10.55	18.81
Total	97.07	99.08	98.45	96.83	94.89	95.89	93.62	97.12	101.27

Table 3. Chemical compositions of IP chondrules.

	1	7	8	8–2	8–3	12	19	40	42	45	46	47	48
Na_2O	0.94	0.87	0.34	0.35	0.35	0.46	0.13	1.12	0.30	0.04	0.64	0.60	1.11
MgO	26.57	32.34	43.20	33.24	36.97	41.52	40.04	30.07	26.77	49.20	35.37	30.45	26.64
Al_2O_3	4.84	5.51	1.51	1.38	2.51	3.05	2.26	4.86	1.24	0.89	3.79	2.53	5.43
SiO_2	53.16	48.13	41.15	53.55	45.41	42.91	47.62	46.85	51.11	39.06	49.01	53.39	48.31
K_2O	0.06	0.07	0.02	0.02	0.02	0.03	0.02	0.10	0.00	0.00	0.06	0.06	0.11
CaO	5.12	4.89	1.20	2.13	1.93	2.48	1.86	3.98	3.49	0.38	3.24	4.01	4.74
TiO_2				0.00	0.00				0.11	0.00			
Cr_2O_3													
MnO	0.39	0.18	0.12			0.17	0.42	0.24			0.19	0.22	0.13
FeO	7.20	5.80	7.02	9.07	12.20	9.39	7.32	10.80	12.81	8.25	8.13	5.16	8.94
Total	98.28	97.79	94.57	99.75	99.39	100.00	99.67	98.02	95.83	97.82	100.43	96.42	95.41

	49	50	51–6	54	57	58	60	61	62	64	65	66	67
Na_2O	0.65	0.36	0.40	0.84	0.20	0.40	0.57	1.84	1.10	0.49	0.41	0.56	0.41
MgO	29.53	39.80	32.00	39.43	39.58	36.12	37.11	18.41	26.64	31.66	30.07	39.78	34.92
Al_2O_3	4.14	2.36	2.95	3.83	1.76	3.28	1.95	7.54	6.57	2.95	5.62	2.54	3.98
SiO_2	42.09	46.30	53.84	43.68	40.18	44.16	50.56	52.16	44.05	46.73	55.10	45.42	51.54
K_2O	0.07	0.00	0.01	0.03	0.03	0.00	0.00	0.08	0.03	0.02	0.00	0.00	0.00
CaO	3.19	1.73	2.86	2.94	1.58	2.96	1.87	8.47	4.01	2.39	5.90	2.04	3.71
TiO_2	0.03	0.20	0.04	0.00	0.00	0.05	0.00	0.16	0.03	0.03	0.35	0.00	0.00
Cr_2O_3													
MnO													
FeO	16.84	9.38	6.26	10.50	16.95	11.34	8.35	8.27	18.07	14.34	1.88	7.88	6.26
Total	96.54	100.13	98.37	101.25	100.25	98.31	100.41	96.93	100.50	98.61	99.33	98.22	100.82

	81	303	307	309	314	318	344	369	374	375	386	20
Na_2O	0.26	0.37	0.46	0.23	0.69	0.23	0.68	1.92	0.50	1.00	0.04	1.12
MgO	27.02	38.23	41.87	31.65	32.80	28.95	38.19	16.83	41.66	23.39	35.89	28.19
Al_2O_3	1.09	2.20	3.77	3.42	2.75	1.87	4.03	6.60	3.24	4.80	2.14	13.14
SiO_2	48.05	49.86	41.12	52.01	53.95	54.99	45.33	51.57	41.09	51.32	51.34	42.91
K_2O	0.00	0.05	0.04	0.04	0.08	0.02	0.07	0.12	0.05	0.10	0.01	0.10
CaO	6.06	1.76	3.19	3.30	3.29	4.00	4.10	10.78	2.93	7.32	2.12	7.79
TiO_2	0.10	0.21	0.30	0.28	0.24	0.22	0.21	0.44	0.28	0.42	0.30	
Cr_2O_3	1.05											
MnO												0.12
FeO	13.27	6.59	7.56	6.68	4.76	8.57	9.80	10.45	11.36	6.81	7.52	6.95
Total	96.90	99.27	98.31	97.61	98.56	98.83	102.44	98.71	101.11	95.16	99.36	100.32

Table 4. Chemical compositions of mSP, fSP and unique type chondrules.

	mSP type							unique type	
	23	37	102	319	322	346	397	10–4	29
Na_2O	1.70	1.37	0.85	2.75	2.30	0.98	1.20	1.61	3.02
MgO	36.25	27.66	26.51	21.98	22.13	24.87	39.90	9.45	8.36
Al_2O_3	4.54	2.58	2.14	4.87	3.85	1.86	3.09	8.72	10.16
SiO_2	44.94	55.16	55.57	57.01	54.38	56.44	44.90	58.61	54.15
K_2O	0.02	0.04	0.00	0.04	0.05	0.06	0.05	0.00	0.13
CaO	3.16	3.43	3.51	5.92	7.42	4.23	2.06	13.11	14.46
TiO_2	0.00		0.15	0.32	0.33	0.24	0.35	0.01	
Cr_2O_3			1.25						
MnO		0.57							0.35
FeO	10.09	7.04	8.72	4.73	9.04	9.15	9.11	8.14	3.61
Total	100.70	97.85	98.70	97.62	99.49	97.59	100.66	99.65	94.24

	fSP type									
	38	41	44	301	323	326	339–1	339–2	353	391′
Na_2O	0.91	1.26	1.17	1.12	0.76	1.59	1.82	0.89	0.16	0.32
MgO	26.04	26.20	23.96	21.28	25.17	18.06	22.96	23.66	18.50	20.37
Al_2O_3	2.51	2.11	2.54	1.99	2.01	2.87	3.43	2.04	0.21	0.69
SiO_2	37.73	38.73	37.71	41.46	38.61	42.60	39.39	38.38	45.56	40.44
K_2O	0.06	0.03	0.05	0.02	0.06	0.07	0.05	0.00	0.00	0.00
CaO	1.18	3.07	1.76	2.63	3.87	6.23	3.38	1.85	6.14	6.18
TiO_2				0.24	0.17	0.23	0.37	0.27	0.10	0.12
Cr_2O_3										
MnO	0.40	0.34	0.36							
FeO	30.24	27.95	30.69	29.55	28.00	27.42	26.83	32.43	26.23	28.96
Total	99.07	99.69	98.24	98.29	98.66	99.07	98.23	99.52	96.90	97.08

Table 5. Chemical compositions of devitrified glass fragments. Nos. 80–1, 80–2 and 80–3 are the composition of different parts of a glass fragment.

	80–1	80–2	80–3	32.5	379	352	18′	345	400
Na_2O	0.70	1.14	1.55	6.66	1.63	1.50	0.27	0.98	0.35
MgO	26.94	25.76	26.55	7.65	23.59	20.99	26.90	24.51	27.13
Al_2O_3	1.75	2.51	2.57	10.52	2.83	3.15	0.57	1.79	1.44
SiO_2	31.70	35.16	35.76	48.03	36.37	38.70	37.34	38.12	42.88
K_2O	0.05	0.04	0.02	0.17	0.01	0.17	0.00	0.01	0.04
CaO	0.24	2.55	0.74	14.71	3.51	3.08	0.07	2.85	3.29
TiO_2					0.27	0.31	0.13	0.15	0.22
Cr_2O_3	0.75	0.70	0.56	0.11					
MnO	0.33	0.36	0.30	0.23			0.29		
FeO	34.09	32.28	31.43	7.24	29.10	26.29	33.38	31.21	23.28
Total	96.55	100.49	99.47	95.32	97.31	94.19	98.95	99.62	98.64

Table 6. Chemical compositions of matrix.

	M-1	M-3	M-5	M-7	402
Na_2O	0.12	0.41	0.17	0.11	0.49
MgO	24.05	22.33	24.95	25.57	22.51
Al_2O_3	1.72	1.97	2.32	2.07	2.39
SiO_2	28.08	28.47	29.66	31.18	30.67
K_2O	0.00	0.03	0.00	0.00	0.04
CaO	0.23	0.47	0.52	0.42	0.39
TiO_2	0.08	0.15	0.00	0.09	0.17
Cr_2O_3	0.42	0.45	0.36	0.42	
MnO	0.27	0.31	0.33	0.23	
FeO	32.78	35.17	30.12	30.27	34.57
Total	87.75	89.76	88.42	90.35	91.23

Table 7. Chemical types of chondrules. Ratios are in mole.

$\frac{Al}{Na+K+Al}$ \ $\frac{MgO}{MgO+FeO}$		0.65<	0.65>
>0.65	IP	mIP	fIP
<0.65	SP	mSP	fSP

TiO_2, 0.0–0.4% (Table 2). The normative components of AOI's are represented mainly by olivine with variable amounts of high-Ca pyroxene, anorthite and nepheline.

3.3. The chemical compositions of chondrules also show wide variation: SiO_2, 35–60 wt%; MgO, 8–50%; FeO, 2–33%; Al_2O_3, 0.2–13%; CaO, 0.3–15%; Na_2O, 0.04–3%; and K_2O, 0.00–0.13% (Tables 3 and 4), being represented by the mixtures of normative olivine and pyroxene with relatively constant normative plagioclase. Most chondrules show the mole ratios of $SiO_2/(SiO_2+MgO+FeO)$ between 0.30 and 0.70. But rare chondrules have ratios larger than 0.70, and these chondrules are grouped tentatively into a unique type in this paper. They are chondrules No. 29 and No. 10–4, whose chemical compositions are presented by the mixtures mainly of intermediate plagioclase and high-Ca pyroxene. Common chondrules are classified on the basis of Al/(Al+Na+K) atomic ratios into two types, SP and IP, as shown in Table 7. The SP and IP types are characterized by the normative compositions of sodic (An_{0-30}) and intermediate (An_{30-95}) plagioclase, respectively. Each type is further subdivided into two subtypes on the basis of MgO/(MgO+FeO) mole ratios as shown in Table 7.

3.4. Some devitrified glass fragments are observed in this chondrite. They never show spherical outlines and may be fragments of large glasses or large glassy chondrules. Their chemical compositions are presented in Table 5. They are remarkably similar in chemical composition to the matrix, except glass fragment No. 32.5. Therefore, these devitrified glass fragments may have been formed from materials similar to the matrix by melting prior to or during their accretion onto the chondrite parental body. No. 32.5 fragment shows a chemical composition which is similar to the devitrified groundmass glass of fSP chondrules. Thus it may have derived from the fragmentation of large fSP chondrules.

3.5. Chemical compositions of the matrix were already reported by IKEDA *et al.* (1981), and some additional data are tabulated in Table 6. Chemical compositions of the matrix are relatively uniform, as follows: SiO_2, 27–36 wt%; MgO, 22–30%; Σ FeO, 30–40%; Al_2O_3, 0.6–3.6%; CaO, 0.07–1.8%; Na_2O, 0.1–0.7%; K_2O, 0.00–

0.12%; and Ti_2O, 0.03–0.20%. They are represented by the mixtures mainly of ferrous olivine (Fo_{55-65}) and Fe-bearing minerals (Fe-sulfide, Fe-metal or Fe-oxide) with small amounts of nepheline, spinel and/or high-Ca pyroxene components.

3.6. The chemical compositions of fine to medium-grained CAI's, AOI's, chondrules and matrix are plotted in Figs. 1 to 5. Metal-free and/or metal-bearing solar condensate trends are shown for reference in Figs. 2 to 5. The two trends are constructed

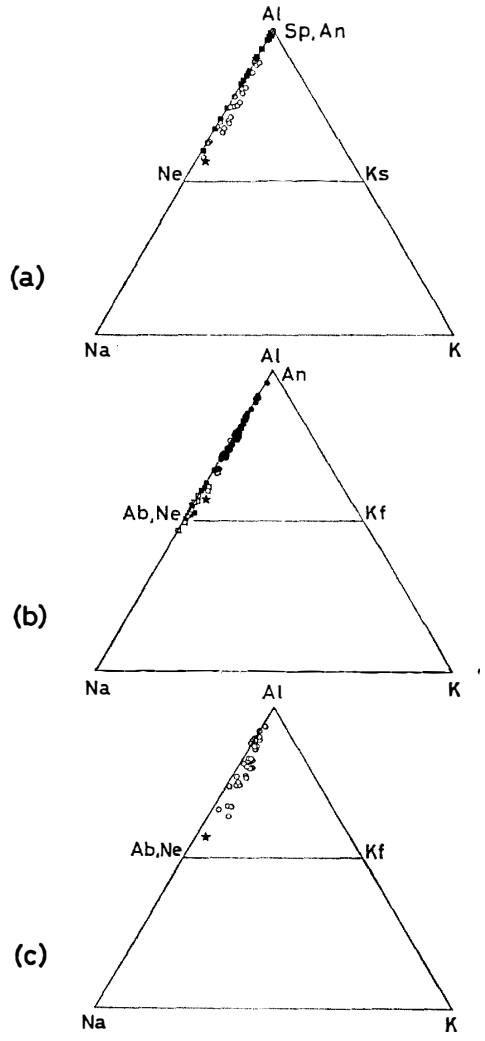

Fig. 1. Atomic plotting of Al-Na-K for the constituent units of ALH-77003. (a): Fine to medium-grained CAI (open circle) and AOI (solid square). (b): Chondrules of chemical types of unique (open circle), mIP (solid circle), mSP (solid square) and fSP (open square). (c): Matrix (open circle). Abbreviations of Sp, An, Ne, Ks, Ab and Kf are spinel, anorthite, nepheline, kalsilite, albite and K-feldspar, respectively. Solid star is the solar abundance (CAMERON, 1973).

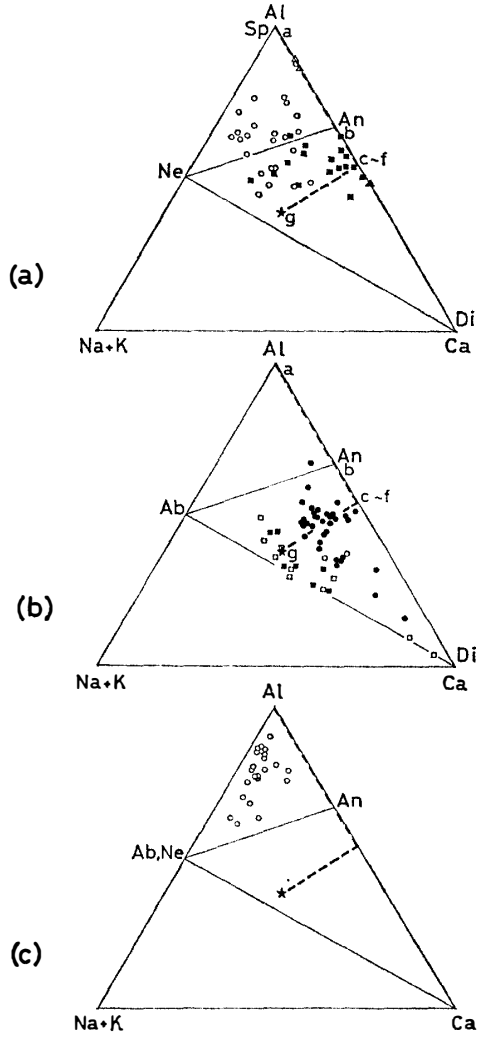

Fig. 2. Atomic plotting of Al-(Na+K)-Ca for the constituent units of ALH-77003. Symbols are the same as in Fig. 1. Di is diopside. The dashed line and small letters show the solar condensate trend (see text).

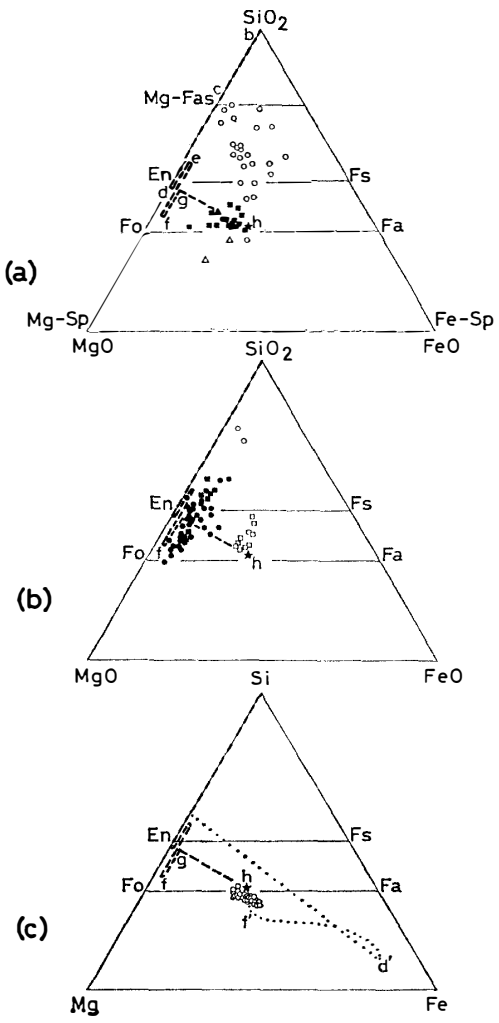

Fig. 3. Molecular plotting of SiO_2-MgO-FeO in (a) and (b) and atomic plotting of Si-Mg-Fe in (c) for the constituent units of ALH-77003. Symbols are the same as in Fig. 1. Abbreviations of Mg-Fas, En, Fs, Fo, Fa, Mg-Sp and Fe-Sp are magnesium fassaite, enstatite, ferrosilite, forsterite, fayalite, magnesium spinel and hercynite, respectively. The dashed and dotted lines are the metal-free and metal-bearing solar condensate trends, respectively (see text).

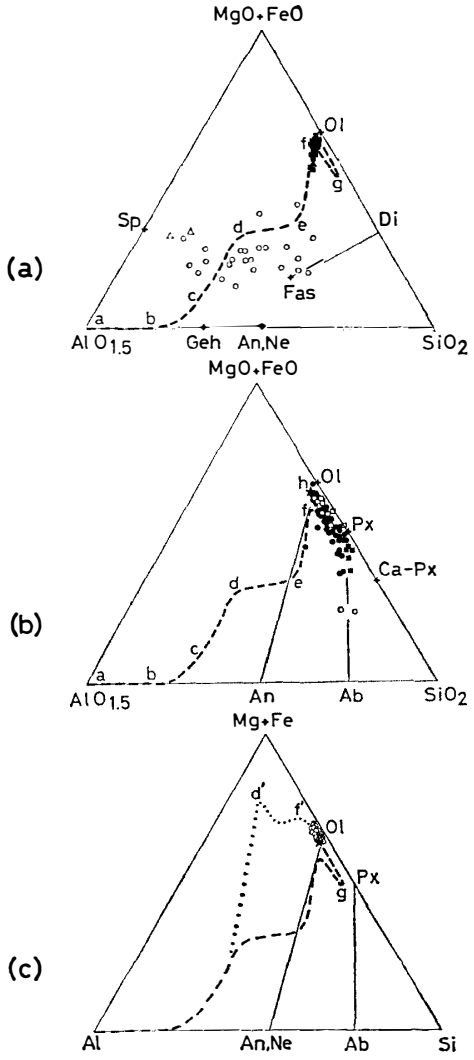

Fig. 4. Molecular plotting of (MgO+FeO)-$AlO_{1.5}$-SiO_2 in (a) and (b) and atomic plotting of (Mg+Fe)-Al-Si in (c) for the constituent units of ALH-77003. Symbols are the same as in Fig. 1. Abbreviations of Ol, Fas, Di, Sp, Geh, An, Ne, Px and Ca-Px are olivine, fassaite, diopside, spinel, gehlenite, anorthite, nepheline, low-Ca pyroxene and high-Ca pyroxene, respectively. The dashed and dotted lines are the same as in Fig. 3.

from the chemical compositions of the solar nebula condensates at several temperatures under the condition of total gas pressure of 10^{-3} atm. The metal-free solar condensate trend corresponds to the silicate and oxide condensates, except metallic Fe. The compositions of the condensates at 1500, 1450 and 1440 K are quoted from GROSSMAN (1975). Those at 1650 and 1362 K are calculated from the data of GROSSMAN and LARIMER (1974). The composition of the condensate at 1000 K is

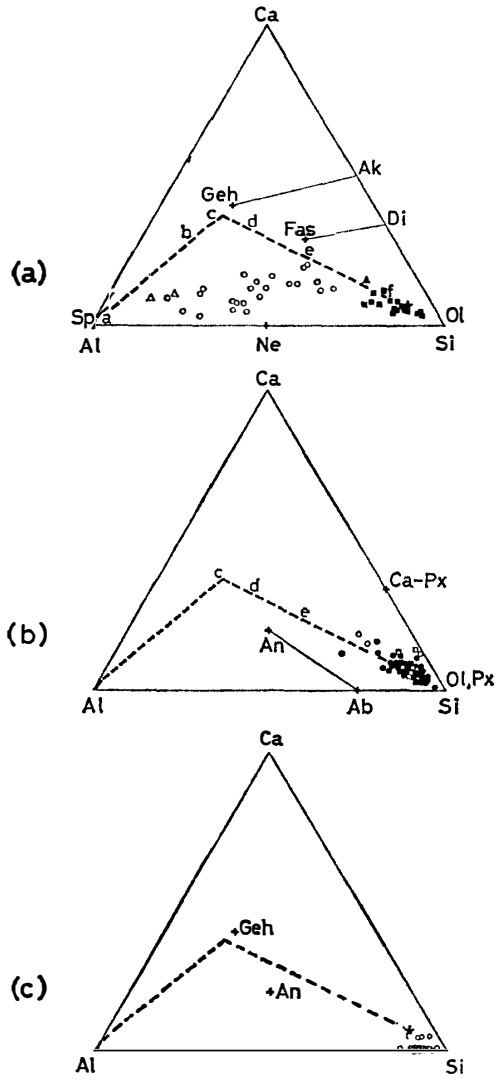

Fig. 5. Atomic plotting of Ca-Al-Si for the constituent units of ALH-77003. The symbols and abbreviations are the same as in Fig. 4. Ak is akermanite. The dashed line is the same as in Fig. 3.

assumed to equal the solar abundance because major components such as Al, Ca, Mg, Si and Na finish their condensation at this temperature. Below 700 K, oxidation and sulfurization of metallic Fe take place, and the condensate is represented by the composition equal to the solar abundances, the metal-bearing trend coinciding with the metal-free trend. Symbols a, b, c, d, e, f, g and h in Figs. 2 to 5 are the chemical compositions of metal-free condensates at 1650, 1600, 1500, 1450, 1440, 1362, 1000 and 700 K, respectively, and d′ and f′ are those of the metal-bearing trend at 1450 and 1362 K, respectively.

Figure 1 shows that the K/(Na+K) ratios of fine-grained CAI's are generally higher than those of AOI's and chondrules, and nearly coincide with those of the matrix and the solar abundances. In Fig. 2, the chondrules are plotted around the solar condensate trend between 1362 and 700 K, the IP type being higher in temperature than the SP type. On the other hand, fine-grained CAI's and AOI's deviate from the high temperature trend toward (Na+K) apex.

The matrix is extremely poor in CaO content, and alkalis are also depleted in the

matrix in comparison with the solar abundances. Figure 3 shows that Fe-Mg ratios of the fine-grained CAI's, AOI's and chondrules are variable. The ratios for chondrules seem to be divided into two groups, magnesian and ferrous. Although the SP type belongs in both groups, the IP chondrules are limited to the magnesian group. It is characteristic that magnesian (mIP and mSP) group contains fairly constant FeO content. The Mg/Si ratios of fine-grained CAI's are low and variable, but those of AOI's, chondrules and matrix are in average equal to the solar abundances. Especially the Mg/Si of the matrix is surprisingly uniform and slightly higher than the solar abundances.

In Fig. 4, the fine-grained CAI's are plotted widely across the solar condensate trend, whereas the AOI's are limited around f. It is recognized that the chemical composition is discontinuous between the fine-grained CAI's and AOI's. In general, Al contents of chondrules are fairly uniform, indicating the constant normative plagioclase content in them. But some unique chondrules show high contents of Al, deviating from the solar trend. These chondrules contain high normative components of plagioclase and high-Ca pyroxene. The Al contents of the matrix are also uniform and slightly lower than the solar abundance.

In Fig. 5, AOI's and chondrules are plotted along the solar condensate trend, whereas fine-grained CAI's and the matrix are fairly depleted in CaO, resulting in their deviation from the trend.

Figures 1 to 5 show that fine-grained CAI's are fairly rich in alkalis and FeO and poor in CaO in comparison with the high temperature solar condensates. The AOI's also contain variable amounts of alkalis and FeO, although they are plotted along the solar condensate trend in Figs. 4 and 5. On the other hand, the mIP and mSP chondrules plot along the metal-free solar condensate trend in the temperature range between 1362 and 1000 K except for their slightly high FeO contents. The fSP chondrules also show the chemical composition of the trend between 1000 and 700 K, although they seem to be discontinuous in chemical composition to the mIP and mSP chondrules. The matrix is poor in alkalis and CaO and slightly poor in Al_2O_3 and SiO_2 in comparison with the solar condensates at temperatures lower than 700 K.

4. Mineralogy

4.1. Inclusions

In fine-grained CAI's, the constituent minerals are too fine to determine the species under the microscope. Those in medium-grained CAI's and rim pyroxenes surrounding some fine to medium-grained CAI's were analyzed using an electron-probe microanalyzer. In a medium-grained CAI (No. 104), nepheline, spinel and high-Ca pyroxene occur in igneous texture (Fig. 7d), and their chemical compositions are shown in Table 8. The K_2O contents of the nephelines are extremely low, and the CaO contents are also lower than those of the Allende meteorite (ALLEN *et al.*, 1980). The FeO contents of spinels are high and the mole ratios of MgO/(MgO+FeO) are about 0.5, whereas the coexisting high-Ca pyroxenes are extremely magnesian, the mole ratios being 0.98 to 0.99. The high-Ca pyroxenes show high Al_2O_3 contents of about 14

Table 8. Chemical compositions of spinel, nepheline, and pyroxene in fine and medium-grained CAI's.

	43′ Sp	104–3 Sp	104–13 Ne	51–3 rimRx	44′ rimPx	104–1 Px	104–4 Px	104–11 Px	104–12 Px	104–5 rimPx	104–6 rimPx
Na_2O	0.08	0.02	19.89	0.05	0.04	0.01	0.00	0.03	0.02	0.01	0.00
MgO	12.24	12.16	0.28	18.05	14.56	12.62	12.82	13.23	13.69	13.23	14.81
Al_2O_3	63.05	61.17	36.21	1.45	10.05	14.67	14.04	14.80	14.29	11.91	7.08
SiO_2	0.30	0.26	41.46	53.35	47.96	47.35	44.74	45.23	44.62	47.34	51.07
K_2O	0.00	0.00	0.25	0.00	0.01	0.00	0.00	0.00	0.03	0.00	0.00
CaO	0.00	0.12	0.42	25.35	25.49	25.04	24.43	24.75	25.17	25.26	24.99
TiO_2		0.00	0.09			1.58	2.22	2.73	0.73	1.72	1.66
Cr_2O_3	0.18	0.92	0.00	0.13	0.16	0.36	0.44	0.33	0.30	0.56	0.36
MnO	0.05	0.11		0.02	0.00	0.00	0.07			0.03	0.00
FeO	22.11	22.32	0.44	0.73	0.86	0.27	0.35	0.25	0.32	0.39	0.59
Total	98.01	97.08	99.03	99.13	99.12	101.90	99.10	101.35	99.15	100.44	100.55

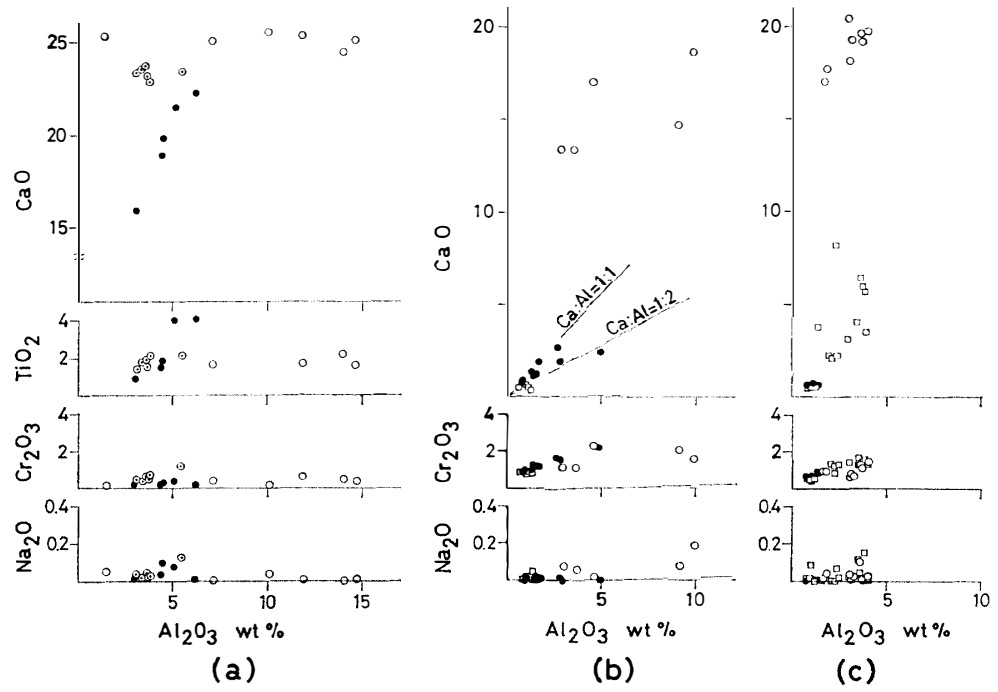

Fig. 6. Chemical compositions (in wt%) of pyroxenes. (a): High-Ca pyroxenes of fine to medium-grained CAI's (open circle), No. 29 chondrule of unique type (open circle with dot) and No. 20 chondrule of mIP type (solid circle). (b): High-Ca pyroxenes (open circle), orthopyroxenes (solid circle) and low-Ca clinopyroxenes (open square) in No. 1 chondrule of mIP. (c): High-Ca pyroxenes (open circle), orthopyroxenes (solid circle) and low-Ca clinopyroxenes (open square) in some mIP chondrules.

to 15 wt% and low TiO_2 contents of 0.7 to 2.7 wt%. The CaO of the pyroxenes are higher than those of chondrules (Fig. 6) because of high contents of Ca-Tschermak molecules in the medium-grained CAI. Rim pyroxenes around fine to medium-grained CAI's show similar chemical compositions to the high-Ca pyroxenes of No.

104 inclusion, but the Al_2O_3 contents of the former are lower, ranging widely from 12 to 1 wt%.

Olivines are a main constituent in AOI's. They are heterogeneous in MgO/(MgO+FeO) mole ratios, ranging from 0.95 to 0.60, although there is a tendency to become more ferrous toward the margins of AOI's.

4.2. Chondrules

Several spinel grains are observed in the central part of No. 20 chondrule (type IP) as shown in Fig. 7b. Their TiO_2 and Cr_2O_3 contents are low (Table 9). They show chemical zoning in MgO/(MgO+FeO) mole ratios from 0.82 in the core to 0.67 in the rim.

Plagioclases are observed in many chondrules of the IP type. In general, they occur interstitial together with high-Ca pyroxenes, which means they are products of the latest stage crystallization in the chondrules. The An contents vary within the range of 60 to 85 mole percent between chondrules and also within a chondrule.

Table 9. Chemical compositions of spinel (Sp) and plagioclase (Pl) in chondrules of Nos. 20 (type IP), 12 (IP), 27 (IP), 25 (IP) and 312 (IP).

	20–1 Sp	20–2 Sp	20–3 Sp	20–5 Sp	20–6 Sp	20–8 Pl	20–9 Pl	20–14 Pl	20–17 Pl	20–18 Pl	20–19 Pl	12–4 Pl
Na_2O	0.01	0.01	0.00	0.01	0.00	2.94	2.99	3.04	2.70	3.06	4.12	2.54
MgO	21.16	22.47	22.48	17.35	19.20	0.72	0.79	0.98	0.83	0.60	1.05	1.15
Al_2O_3	68.20	67.94	67.78	65.48	67.04	32.60	32.98	32.40	33.00	32.77	30.82	32.07
SiO_2	0.06	0.11	0.08	0.17	0.34	45.77	44.92	46.60	45.38	45.77	48.16	47.61
K_2O	0.04	0.02	0.04	0.00	0.02	0.20	0.21	0.29	0.23	0.16	0.33	0.17
CaO	0.00	0.00	0.03	0.04	0.02	16.52	16.55	16.51	16.20	15.90	14.40	16.11
TiO_2	0.34	0.34	0.26	0.43	0.40							
Cr_2O_3	0.15	0.57	0.14	0.22	0.36	0.03	0.04	0.00	0.00	0.05	0.11	0.03
MnO	0.07	0.12	0.13	0.18	0.10	0.03	0.01	0.09	0.06	0.05	0.00	0.03
FeO	10.10	9.29	9.02	16.02	13.13	0.21	0.33	0.57	0.51	0.26	0.82	0.56
NiO	0.10	0.04	0.00	0.15	0.05							
Total	100.23	100.91	99.97	100.05	100.67	99.02	98.83	100.49	98.90	98.64	99.81	100.28

	12–12 Pl	27–7 Pl	27–9 Pl	27–11 Pl	27–14 Pl	27–18 Pl	27–19′ Pl	27–21 Pl	27–29 Pl	25–9 Pl	312–6 Pl	312–9 Pl
Na_2O	1.82	2.79	2.21	2.50	2.25	1.83	2.22	2.20	2.40	3.01	3.96	4.59
MgO	0.69	0.56	0.81	0.46	0.59	0.35	0.47	0.46	0.62	0.99	0.67	0.61
Al_2O_3	33.13	31.62	32.11	33.62	32.64	33.50	32.88	32.90	32.27	31.35	31.20	31.96
SiO_2	45.02	46.80	47.17	45.47	47.04	46.39	45.75	45.94	46.26	47.24	47.92	47.06
K_2O	0.13	0.17	0.05	0.08	0.08	0.04	0.15	0.08	0.08	0.25	0.19	0.34
CaO	16.88	16.09	15.94	17.05	16.50	17.58	15.91	17.12	16.48	14.61	14.33	14.36
TiO_2												
Cr_2O_3	0.00	0.08	0.09	0.06	0.00	0.14	0.05	0.23	0.17	0.00	0.00	0.05
MnO	0.04	0.04	0.24	0.05	0.00	0.12	0.04	0.02	0.00	0.18	0.02	0.14
FeO	0.53	0.37	0.67	0.51	0.36	0.40	0.56	0.67	0.66	1.09	0.91	0.74
NiO												
Total	98.24	98.51	99.29	99.79	99.46	100.35	98.04	99.60	98.94	98.72	99.21	99.86

The Or contents are lower than 2 mole%. The SiO_2 contents of plagioclases are slightly lower than stoichiometric composition, which means that they contain small amounts of nepheline component in solid solution.

Pyroxens are the main constituent mineral in unique, mIP and mSP chondrules, although they never occur in fSP chondrules. Their chemical compositions are tabulated in Table 10 and shown in Fig. 6. They are high-Ca pyroxene, low-Ca clinopyroxene and orthopyroxene. Two types of low-Ca clinopryoxenes seem to occur, one being primary clinopyroxene and the other being inverted protopyroxene. High-Ca pyroxenes of No. 29 chondrule (unique type) are nearly pure diopside. The high-Ca pyroxenes of No. 20 chondrule (IP type) show chemical zoning from CaO- and TiO_2-poor core to CaO- and TiO_2-rich rim (Fig. 6a). In Fig. 6b, the chemical compositions of high-Ca pyroxene, orthopyroxene and low-Ca clinopyroxene showing polysynthetic twinning in No. 1 chondrule (IP type) are shown. The low-Ca clinopyroxene is lower in CaO and Cr_2O_3 contents than the orthopyroxene. The former shows a dirty appearence under the microscope whereas the latter is clean euhedral crystals (Fig. 7c). The orthopyroxenes show chemical zoning from CaO- and Cr_2O_3-poor core to rich rim, and they plot above the line of Ca/Al=1/2 as shown in Fig. 6b, indicating that the CaO contents form both the diopside and Ca-Tschermak molecules in solid solution. Pyroxenes of several other mIP chondrules are plotted together in Fig. 6c. There is no systematic difference in Cr_2O_3 content between high-Ca pyroxene, orthopyroxene and low-Ca clinopyroxene, but the Na_2O contents of orthopyroxenes are always lower than other pyroxenes. When low-Ca clinopyroxenes crystallize prior to orthopyroxenes, the former show polysynthetic twininng and are lower in CaO content (less than 1 wt%) than the latter, although low-Ca clinopyroxenes show high CaO content up to 8 wt% when orthopyroxenes do not occur. The extremely low-Ca clinopyroxenes crystallizing prior to orthopyroxenes are considered to be inverted protopyroxenes.

Olivines are a main constituent in chondrules. They also occur rarely as rims around small chondrules. In olivines of all mIP and mSP chondrules, the mole ratios of MgO/(MgO+FeO) range from 0.995 to 0.65, and they often show remarkable compositional zoning from magnesian cores to ferrous rims. On the other hand, the olivines of fSP chondrules are fairly uniform (about $Fo_{65}Fa_{35}$) or show slight Mg-Fe zoning. Rim olivines around some small chondrules are heterogeneous in MgO/(MgO+FeO) mole ratios and generally more ferrous than olivines in chondrules.

Groundmass glasses represent the latest stage residual liquid of the crystallization of chondrules. Their chemical compositions are tabulated in Table 11. They contain high normative contents of plagioclase and high-Ca pyroxene. Generally, the groundmass glasses in IP and SP chondrules show the same atomic ratios of Al/(Al+Na+K) as the chondrules. Thus the classification between the types IP and SP can be done from the chemical compositions of their groundmass glasses, except for some delicate chondrules.

4.3. Mineral fragments

Silicate mineral fragments occur in the matrix and they are mainly olivine, orthopyroxene and low-Ca clinopyroxene. Their chemical compositions are nearly the

Table 10. Chemical compositions of pyroxenes in chondrules, No. 29 (unique type), No. 20 (IP), No. 1 (IP), No. 28 (IP), No. 27 (IP), No. 19 (IP), No. 12 (IP), No. 25 (IP) and 23 (mSP). Opx, Cpx and CaPx are orthopyroxene, low-Ca clinopyroxene and high-Ca clinopyroxene, respectively.

	29–1 CaPx	29–4 CaPx	29–5 CaPx	29–6 CaPx	29–13 CaPx	29–14 CaPx	20–10 CaPx	20–11 CaPx	20–35 CaPx	20–37 CaPx	20–39 CaPx	1–5 Opx	1–8 Opx	1–9 Opx	1–12 Opx	1–13 Opx
Na_2O	0.04	0.03	0.02	0.05	0.03	0.13	0.10	0.01	0.40	0.08	0.02	0.02	0.03	0.00	0.03	0.00
MgO	17.55	17.01	17.37	17.44	17.40	16.40	21.24	16.87	21.40	17.18	24.36	32.19	35.59	35.91	35.89	31.31
Al_2O_3	3.12	3.77	3.38	3.61	3.64	5.54	4.45	6.21	4.41	5.10	2.98	2.66	1.42	0.81	0.86	4.93
SiO_2	51.89	51.18	52.28	51.63	52.02	49.64	52.35	51.54	52.38	51.76	53.56	55.02	55.72	57.04	56.36	52.38
K_2O	0.05	0.03	0.03	0.05	0.08	0.06	0.02	0.20	0.03	0.04	0.02	0.00	0.00	0.00	0.00	0.00
CaO	23.26	22.86	23.46	23.60	23.09	23.36	19.80	22.18	18.87	21.43	16.89	2.61	1.10	0.76	0.80	2.38
TiO_2	1.39	2.15	1.84	1.89	1.59	2.22	1.92	4.12	1.54	4.05	0.97					
Cr_2O_3	0.51	0.70	0.41	0.58	0.51	1.21	0.31	0.17	0.18	0.40	0.20	1.65	1.32	0.90	1.00	2.19
MnO	0.36	0.31	0.40	0.26	0.27	0.45	0.18	0.04	0.14	0.01	0.08	0.83	0.17	0.17	0.16	0.68
FeO	0.54	0.51	0.49	0.37	0.30	0.41	0.30	0.19	0.97	0.24	0.74	4.61	4.77	4.40	4.16	4.45
NiO	0.24	0.01	0.02	0.03	0.00	0.00	0.04	0.09	0.05	0.00	0.00					
Total	98.94	98.56	99.69	99.51	98.93	99.42	100.70	101.43	100.01	100.28	99.83	99.58	100.12	100.00	99.27	98.31

	1–16 CaPx	1–18 CaPx	1–19 CaPx	1–20 Opx	1–22 Opx	1–23 Opx	1–24 CaPx	1–29 Opx	1–30 CaPx	1–51 Cpx	1–53 Cpx	1–54 Cpx	1–55 Cpx	27–5 CaPx	27–10 CaPx	27–20 CaPx
Na_2O	0.08	0.19	0.08	0.00	0.00	0.01	0.06	0.02	0.02	0.00	0.01	0.05	0.02	0.03	0.10	0.01
MgO	18.87	15.74	22.51	34.58	33.11	35.31	22.53	33.19	19.67	38.00	38.11	37.41	37.19	20.73	20.70	21.97
Al_2O_3	9.08	9.92	2.91	1.34	2.77	1.41	3.57	1.72	4.55	0.73	1.16	1.25	1.11	3.97	3.56	3.64
SiO_2	48.59	48.54	52.33	57.07	54.88	56.57	52.37	55.73	52.01	58.00	57.27	57.14	57.31	54.06	51.61	53.50
K_2O	0.00	0.00	0.00	0.00	0.00	0.00	0.00	0.00	0.00	0.03	0.00	0.00	0.00	0.00	0.00	0.00
CaO	14.71	18.67	13.37	1.27	1.89	1.17	13.31	1.81	16.99	0.49	0.53	0.39	0.49	19.74	19.59	19.14
TiO_2										0.07	0.00	0.18	0.07			
Cr_2O_3	2.06	1.65	1.13	1.01	1.55	1.24	1.05	1.20	2.33	0.90	0.85	0.83	0.77	1.40	1.26	1.08
MnO	0.85	0.92	0.83	0.13	0.42	0.19	1.04	0.38	0.77					0.05	0.21	0.21
FeO	4.78	3.15	4.61	5.14	4.28	3.92	4.29	5.46	3.35	3.55	3.76	4.13	4.17	1.01	0.90	0.86
NiO																
Total	99.02	98.76	97.78	100.57	98.91	99.81	98.22	99.51	99.70	101.77	101.69	101.38	101.12	100.98	97.92	100.41

Table 10 (continued).

	27–22 Opx	27–23 CaPx	27–11 Cpx	27–02 Cpx	25–3 Opx	25–5 Opx	25–8 CaPx	28–6 Cpx	28–8 Cpx	28–9 Cpx	28–10 Cpx	28–11 Cpx	28–12 Cpx	28–13 Cpx	28–01 Cpx	28–02 Cpx
Na_2O	0.00	0.01	0.09	0.01	0.00	0.00	0.04	0.01	0.03	0.13	0.16	0.01	0.02	0.00	0.00	0.05
MgO	38.64	22.03	39.33	39.48	38.56	39.02	21.75	30.86	33.07	32.53	31.10	33.41	35.12	35.34	35.70	30.21
Al_2O_3	1.29	1.64	1.02	0.75	0.94	0.74	1.84	3.74	2.98	3.54	3.77	3.96	2.41	2.20	2.07	3.54
SiO_2	56.55	54.07	58.55	58.43	57.03	58.27	54.67	53.90	56.39	55.06	54.83	54.39	57.05	56.51	58.21	55.51
K_2O	0.00	0.00	0.00	0.00	0.03	0.02	0.01	0.05	0.03	0.04	0.07	0.03	0.04	0.01	0.00	0.01
CaO	0.60	19.69	0.70	0.48	0.63	0.56	17.67	6.01	3.08	3.94	5.69	3.39	2.20	2.10	2.27	6.42
TiO_2			0.30	0.32				0.48	0.34	0.55	0.48	0.32	0.26	0.26	0.28	0.44
Cr_2O_3	0.90	0.91	0.48	0.56	0.64	0.59	0.91	1.56	1.42	1.67	1.59	1.41	1.35	1.27	1.23	1.35
MnO	0.09	0.27			0.04	0.08	0.26	0.47	0.25	0.45	0.38	0.33	0.30	0.02		
FeO	0.56	0.71	1.06	1.08	1.04	1.11	1.14	2.08	2.55	2.40	2.01	2.24	2.36	2.30	2.10	2.58
NiO								0.00	0.16	0.01	0.00	0.12	0.02	0.00		
Total	98.63	99.32	101.53	101.11	98.92	100.39	98.28	99.16	100.27	100.30	100.09	99.61	101.13	100.20	101.87	100.10

	19–2 CaPx	19–3 Opx	19–4 Opx	19–7 Opx	19–9 CaPx	19–10 Opx	12–2 Cpx	12–8 Cpx	12–10 Cpx	12–03 Cpx	23–4 Opx	23–6 CaPx	23–8 Opx	23–9 CaPx	23–01 Cpx	23–02 Cpx
Na_2O	0.04	0.01	0.02	0.01	0.02	0.03	0.06	0.01	0.00	0.02	0.00	0.06	0.00	0.04	0.03	0.02
MgO	22.38	35.68	35.63	36.01	15.88	35.39	31.18	38.96	38.70	36.46	39.82	18.63	39.97	19.14	39.48	39.01
Al_2O_3	6.31	2.09	1.60	1.80	14.34	2.03	2.18	0.91	1.11	1.39	1.26	9.21	1.36	7.89	1.01	1.31
SiO_2	51.81	56.31	56.98	56.29	45.63	56.46	55.98	57.93	57.17	57.74	57.75	49.14	57.88	50.69	58.77	58.26
K_2O	0.00	0.00	0.00	0.00	0.00	0.00	0.05	0.05	0.05	0.00	0.00	0.00	0.01	0.00	0.00	0.00
CaO	15.49	1.15	1.35	1.31	19.06	1.51	8.12	0.49	0.52	3.86	0.49	21.12	0.56	20.29	0.47	0.46
TiO_2										0.46	0.17	0.88	0.32	0.84	0.23	0.28
Cr_2O_3	0.40	1.31	1.21	1.39	0.65	1.12	0.84	0.53	0.55	0.94	0.35	1.19	0.43	1.31	0.37	0.62
MnO	0.59	0.98	0.00	0.15	0.79	0.17	0.07	0.00	0.05							
FeO	4.47	3.62	3.95	4.77	2.62	3.44	1.05	1.13	1.22	1.02	0.46	0.37	0.69	0.42	0.74	1.31
NiO																
Total	101.49	101.15	100.73	101.73	98.99	100.14	99.54	100.01	99.37	101.90	100.31	100.59	101.22	100.63	101.10	101.25

Table 11. Chemical compositions of groundmass glasses in chondrules, No. 29 (unique type), No. 1 (IP), No. 19 (IP), No. 23 (mSP) and No. 36 (fSP).

	29–3	29–8	29–10	29–11	19–12	29–15	29–17	29–19	29–102	29–103
Na_2O	5.65	6.97	8.12	6.41	6.59	6.64	6.30	7.55	7.07	5.67
MgO	3.74	5.56	3.22	3.91	2.24	3.48	5.40	3.76	7.99	5.14
Al_2O_3	17.13	16.30	16.16	16.74	17.48	17.47	16.05	16.90	15.95	16.18
SiO_2	56.11	48.45	47.07	57.80	57.48	57.60	52.67	47.52	49.91	53.13
K_2O	0.08	0.41	1.16	0.13	0.12	0.28	0.51	1.10	0.72	0.11
CaO	12.41	12.19	12.67	10.84	9.31	11.18	13.59	12.81	12.06	13.55
TiO_2	0.26	0.27	0.32	0.32	0.33	0.30	0.17	0.32		
Cr_2O_3	0.12	0.08	0.06	0.05	0.10	0.11	0.07	0.00	0.14	0.18
MnO	0.10	0.17	0.15	0.19	0.11	0.08	0.09	0.20	0.13	0.19
FeO	3.68	9.15	10.44	2.89	3.53	3.72	4.12	9.26	7.66	4.34
NiO	0.00	0.00	0.04	0.00	0.00	0.08	0.01	0.01		
Total	99.29	99.55	99.41	99.29	97.28	100.94	99.00	99.44	101.63	98.50

	29–104	29–105	29–106	29–107	29–Gm	1–4	1–10	1–21	1–31	1–101
Na_2O	6.50	8.56	8.28	7.92	6.16	3.83	3.65	4.08	4.05	7.05
MgO	3.56	5.00	5.02	4.29	3.70	4.16	4.81	4.98	4.40	5.36
Al_2O_3	17.25	17.52	17.54	15.76	16.98	19.01	19.89	20.74	19.11	18.55
SiO_2	53.84	46.45	45.64	45.08	58.10	52.88	51.04	52.16	53.95	45.40
K_2O	0.18	1.20	1.14	1.06	0.03	0.04	0.10	0.12	0.09	0.77
CaO	11.16	9.24	12.36	12.47	10.99	13.41	13.17	12.33	12.51	11.23
TiO_2					0.44					
Cr_2O_3	0.15	0.02	0.09	0.74	0.10	0.21	0.38	0.20	0.22	0.21
MnO	0.08	0.10	0.01	0.17	0.01	0.62	0.44	0.54	0.46	0.79
FeO	4.14	10.44	8.39	9.63	3.21	5.01	4.32	4.21	3.97	6.41
NiO										
Total	96.87	98.53	98.48	97.11	99.71	99.17	97.80	99.36	98.76	95.77

	1–102	1–103	1–104	1–105	1–106	1–107	1–G1	1–G2	19–1	19–8
Na_2O	4.28	3.62	3.80	3.48	8.58	3.84	4.00	3.55	2.52	2.70
MgO	4.37	4.32	4.82	4.40	5.04	4.41	5.00	5.10	7.68	7.97
Al_2O_3	18.16	18.67	18.76	19.63	18.51	18.29	21.27	19.18	23.09	24.63
SiO_2	50.41	53.65	51.53	53.73	45.80	52.33	52.11	52.60	51.18	48.81
K_2O	0.21	0.09	0.07	0.04	1.20	0.11	0.12	0.07	0.00	0.08
CaO	13.09	13.80	13.25	12.84	11.49	13.20	12.38	12.94	12.51	12.53
TiO_2							0.73			
Cr_2O_3	0.18	0.17	0.18	0.17	0.25	0.12	0.09	0.35	0.22	0.30
MnO	0.80	0.74	0.66	0.90	0.84	0.74	0.46	0.63	0.42	0.55
FeO	4.84	4.89	5.41	4.42	6.27	5.72	3.96	4.18	2.45	2.97
NiO										
Total	96.34	99.96	98.47	99.60	97.99	98.74	100.14	98.60	100.12	100.55

	23–5	23–7	23–10	23–13	36–2	36–3	36–4	36–5	36–6
Na_2O	12.66	12.18	12.95	13.04	7.90	8.02	8.29	8.18	7.97
MgO	3.16	3.97	3.30	3.45	6.40	7.52	6.99	7.79	6.20
Al_2O_3	23.29	22.50	23.64	23.80	13.45	12.78	13.49	13.23	13.39
SiO_2	51.76	51.54	53.74	52.17	48.27	46.51	47.70	45.45	46.51
K_2O	0.34	0.34	0.33	0.45	0.18	0.13	0.09	0.09	0.07
CaO	5.24	5.97	5.57	5 29	11.58	10.07	10 29	9.28	11.08
TiO_2	0.18	0.01	0.15	0.13					
Cr_2O_3	0.26	0.30	0.16	0.05	0.21	0.17	0.12	0.09	0.16
MnO					0.21	0.15	0.25	0.20	0.48
FeO	0.97	1.33	1.65	1.56	11.85	11.87	12.73	12.53	11.13
NiO									
Total	99.87	98.13	101.48	99.94	100.05	97.22	99.95	96.84	96.99

same as those in chondrules, showing that most of them were derived from the disaggregation of chondrules. Opaque minerals occur as fragments set in the matrix. They are kamacite, taenite and/or troilite. Some opaque mineral grains have a rim of olivines. The chemical compositions of the olivines are the same as those in AOI's and the rim olivines around some small chondrules, indicating that the rim olivines around the opaque mineral grains and small chondrules formed under the similar conditions to the AOI's.

5. Crystallization of Chondrules

In general, chondrules are thought to crystallize from silicate melt droplets under rapid cooling conditions. In comparison with mSP chondrules, mIP chondrules tend to show higher crystallinity, and this means that the cooling rates of chondrules are systematically different between the mIP and mSP chondrules. In addition, relic minerals are often observed in mIP chondrules whereas they are rare in mSP chondrules. The fSP type also shows low crystallinity in comparison with the mIP type. The most fSP chondrules consist of euhedral olivine grains and black devitrified glasses, completely lacking in pyroxenes. Some small fSP chondrules are made up only of devitrified glass. Therefore, the average crystallinity of fSP seems to be slightly lower than that of mSP. Several examples of the crystallization of typical chondrules of unique, mIP, mSP and fSP types are as follows, but the crystallization of opaque minerals is not dealt with in this paper.

5.1. No. 29 chondrule (unique type)

This chondrule is spherical and about 230 microns in diameter, consisting of euhedral diopside crystals and groundmass glass (Fig. 7a). The chemical compositions of diopsides and glass are tabulated in Tables 10 and 11, respectively, and shown in Fig. 8. The groundmass glass in the peripheral part is dark whereas the inner glass is clean and transparent. The clean glass shows some variation in chemical composition, and the glass in contact with diopside crystals is more depleted in diopside molecules in comparison with the clean glass far from the diopside crystals. This is shown by the dashed line in Fig. 8 and may be due to the rapid crystallization of diopside crystals. The dark glass in the peripheral part shows strange chemical zonation within about 40 microns width in the rim. The Na_2O and K_2O contents increase toward the rim from about 6 wt% and 0.1 wt% up to 10% and 2%, respectively, as shown in Fig. 9. The Fe contents also increase from about 3.5 wt% to more than 10% as FeO, whereas the SiO_2 contents decrease from about 57 wt% to less than 44%. The Al_2O_3 contents are constant between 16 and 18 wt%. This chemical zonation of the dark glass may have formed after the crystallization of the chondrule and the formation of the clean glass, because the diopside crystals in contact with the dark glass have the same chemical composition as those in contact with the clean glass. The high alkali contents of the dark glass can not be explained by the derivation of those components from the surrounding matrix, because the matrix has Na_2O contents less than 0.5 wt% and K_2O less than 0.12 wt% and because the devitrified glass fragments mentioned in the Sections 3–4 never show such a zonation although they are in contact with the matrix. The chemical zonation of the dark glass is thought to

have formed by the introduction of alkalis and FeO and the loss of SiO_2 and CaO during the period after the consolidation of this chondrule and prior to the accretion onto the parental body of the ALH-77003 chondrite.

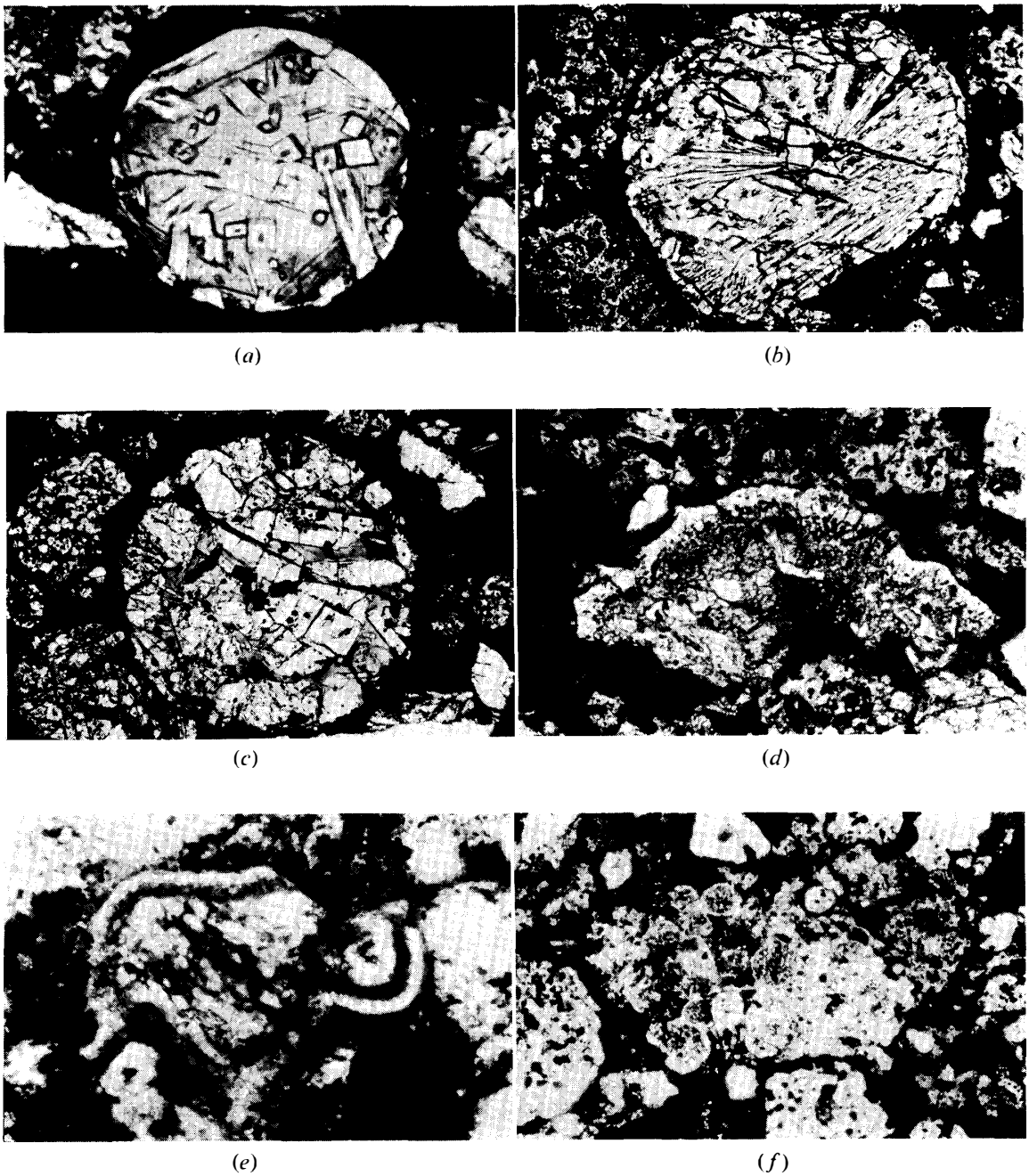

Fig. 7. Photomicrographs of chondrules and inclusions in ALH-77003. (a): No. 29 chondrules of unique type. Long dimension is about 400 microns. (b): No. 20 chondrule of mIP. Long dimension is about 1100 microns. (c): No. 1 chondrule of mIP. Long dimension is about 1100 microns. (d): No. 104 medium-grained CAI. Long dimension is about 500 microns. (e): No. 43' fine to medium-grained CAI. Long dimension is about 200 microns. (f): A botryoidal olivine inclusion of No. 68. Long dimension is about 900 microns.

5.2. No. 20 chondrule (IP type)

This shows circular outline about 800 microns in diameter, and holocrystalline texture (Fig. 7b), consisting of spinel, olivine, high-Ca clinopyroxene and plagioclase. Their chemical compositions are tabulated in Tables 9 and 10. Spinel grains occur in the central part of this chondrule and show subhedral forms of about 50 to 100 microns in size. They zone in MgO/(MgO+FeO) mole ratios from 0.82 in the core to 0.67 in the rim. Olivines occur as barred crystals in one half and euhedral phenocrystic crystals in the other half of this chondrule. Their MgO/(MgO+FeO) ratios are nearly constant at the ratio of 0.99 but the olivines become ferrous in the peripheral part down to 0.67. High-Ca clinopyroxenes occur as rim pyroxene surrounding the chondrule and as needle pyroxene radiating from the central spinel grains. These pyroxenes are extremely magnesian, but a systematic difference in chemical composition is recognized between the rim pyroxene and the needle pyroxene. The latter is rich in CaO, Al_2O_3 and TiO_2 and the former is slightly richer in SiO_2 and FeO. Plagioclases fill interstitial spaces between the barred olivines or occur as radiating crystals

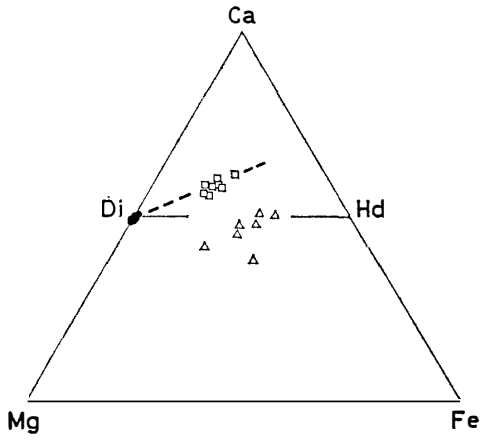

Fig. 8. Chemical compositions of high-Ca pyroxenes (solid circle) and clean groundmass glass (open square) in the No. 29 chondrule. Open triangles are the composition of dark glass of the peripheral part of the chondrule. The dashed line is the fractionation trend of the clean glass. Abbreviations Di and Hd are diopside and hedenbergite.

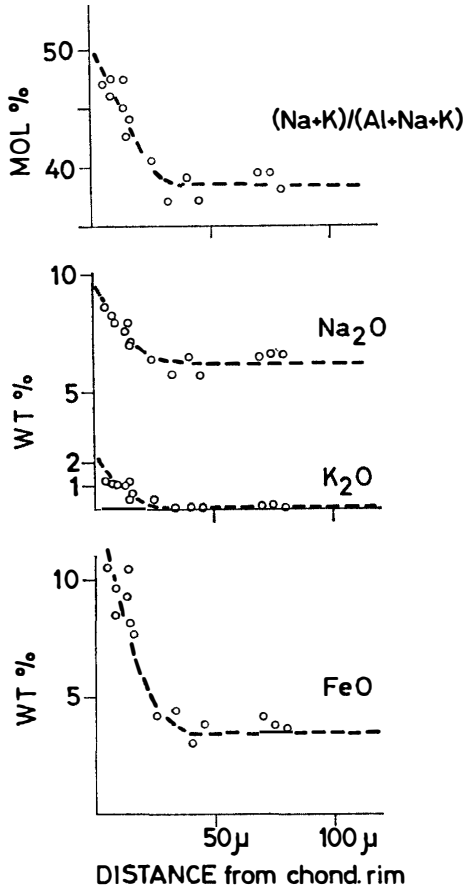

Fig. 9. Chemical compositions of the clean groundmass and peripheral dark glasses in the No. 29 chondrule are plotted against the distance from the chondrule rim. Total Fe contents of the groundmass glasses are shown as FeO wt%.

with pyroxene needles. The crystallization sequence of this chondrule is as follows: Firstly spinel grains crystallized, and next olivines formed the bar and phenocrystic crystals in either half of this chondrule. Finally, plagioclases and high-Ca clinopyroxenes crystallized between the spinel and olivine crystals.

5.3. No. 1 chondrule (IP type)

This chondrule shows spherical form about 700 microns in diameter and consists of olivine, low-Ca clinopyroxene, orthopyroxene, high-Ca clinopyroxene and groundmass glass (Fig. 7c). Their chemical compositions are tabulated in Tables 10 and 11, and shown in Fig. 10. Olivines occur as corroded grains included in low-Ca clinopyroxenes. Olivines show compositional zoning of MgO/(MgO+FeO) ratios from 0.89 to 0.78. Low-Ca clinopyroxenes occur always in the peripheral part of this chondrule and show polysynthetic twinning. They are magnesian and poorer in CaO content than orthopyroxenes (Fig. 10), and are thought to have inverted from protoenstatite. Orthopyroxenes occur as large phenocrysts in the central part of the chondrule, and never contain olivine grains. High-Ca clinopyroxenes occur as needle crystals in the groundmass glass. The crystallization of these pyroxenes is shown schematically in Fig. 11, where several solidus curves of magnesian pyroxenes crystallizing under rapid-cooling conditions are shown in the phase diagram of the enstatite-diopside binary system. The pyroxene crystallization of this chondrule is well represented by the solidus curve of D in Fig. 11, showing the crystallization of primary protoenstatite followed by orthopyroxene and the final crystallization of diopsidic clinopyroxene. The groundmass glass is pale brownish clean glass in the central part and dark dirty glass in the peripheral part of this chondrule. The clean glass in contact with high-Ca clinopyroxene crystals is slightly depleted in the pyroxene molecules in comparison to the clean glass far from the crystals, as shown by the dashed line in Fig. 10a.

Chemical trend of the residual liquid of this chondrule is shown in Fig. 10b. The bulk composition of this chondrule is shown by the large open circle, which corresponds to the melt composition prior to its crystallization. First crystallizing phase was olivine, and the crystallization of olivine changed the melt composition toward the olivine-depleted direction. Around the boundary of olivine and pyroxene liquidus fields the reaction between the olivines and the liquid to produce protopyroxenes took place, and the olivines lost their euhedral forms to be included by the protopyroxene crystals. Then the protopyroxene crystals were removed toward the rim of the droplet by the force of surface tension of the melt droplet. Next, orthopyroxenes crystallized in the central part, and the composition of the residual liquid changed toward the pyroxene-depleted direction, as shown by the dashed line in Fig. 10b. In the last stage, small needles of high-Ca clinopyroxenes crystallized. The residual liquid was rich in FeO in the last stage, and the olivine grains included in pyroxenes became ferrous by the exchange reaction with the residual liquid through cracks or twin boundaries in the host pyroxenes, whereas the pyroxenes preserved their magnesial nature because of low diffusivity in them. The residual liquid was finally quenched as pale brown clean glass in rapid-cooling condition. Protopyroxenes inverted to low-Ca clinopyroxenes showing polysynthetic twinning during or after the crystallization.

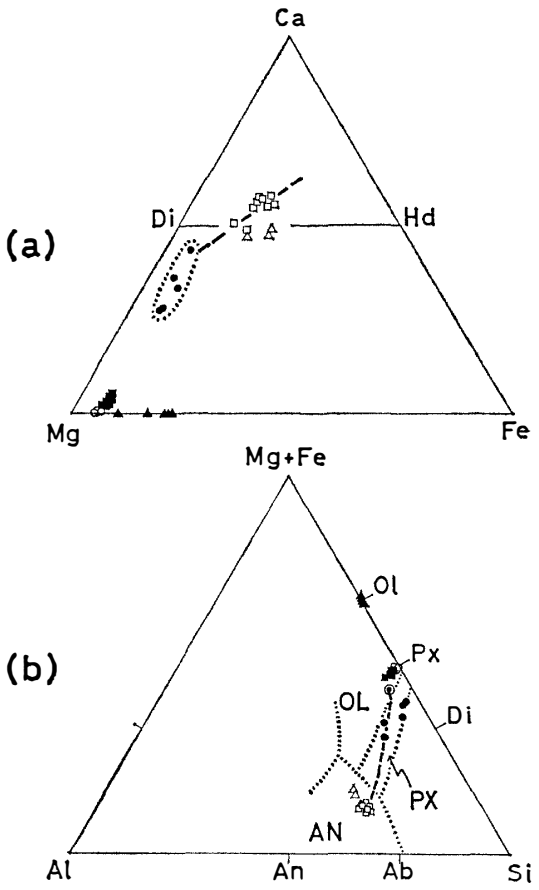

Fig. 10. Atomic plotting of Ca-Mg-Fe in (a) and (Mg+Fe)-Al-Si in (b) for olivine (solid triangle), low-Ca clinopyroxene (open circle), orthopyroxene (solid square), high-Ca pyroxene (solid circle), groundmass glass (open square) and peripheral dark glass (open triangle) in No. 1 chondrule. Dotted lines in (b) are liquidus phase boundaries of the forsterite-anorthite-quartz system quoted from LEVIN *et al. (1964). A large open circle with a dot is the composition of the bulk chondrule. The dashed line in (b) is the trend of the residual liquid by the fractional crystallization of olivines and pyroxenes. Abbreviations of Di, Hd, Ol, Px, Di, An and Ab are diopside, hedenbergite, olivine, low-Ca pyroxene, diopside, anorthite and albite, respectively. OL, PX and AN are the liquidus phase fields of olivine, protoenstatite and anorthite, respectively.*

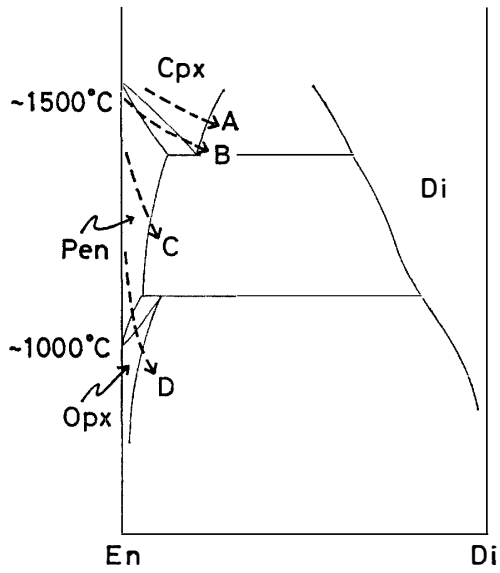

Fig. 11. Temperature-composition diagram showing schematic phase relations of enstatite-diopside binary system quoted from BOYD *and* SCHAIRER *(1964) with slight modification. Cpx, Pen, Opx and Di are stable fields of high-clinopyroxene, protoenstatite, orthopyroxene and diopside, respectively. Dashed lines with arrows are schematic solidus curves of the psuedobinary system of En-Di for the rapid undercooling crystallization of magnesian pyroxenes in mIP and mSP chondrules.*

The dark dirty glass in the peripheral part of the chondrule shows chemical zonation like the No. 29 chondrule. As shown in Fig. 12, the alkalis and FeO contents increase toward the rim and the SiO_2 and CaO contents decrease remarkably, whereas the Al_2O_3 contents are constant at about 19 to 21 wt%. As for the No. 29

chondrule, during the period after the consolidation of this chondrule and prior to the accretion onto the parental body, it may have been brought into the gas rich in alkalis and FeO, changing the composition of the marginal glass to the dark dirty glass around this chondrule.

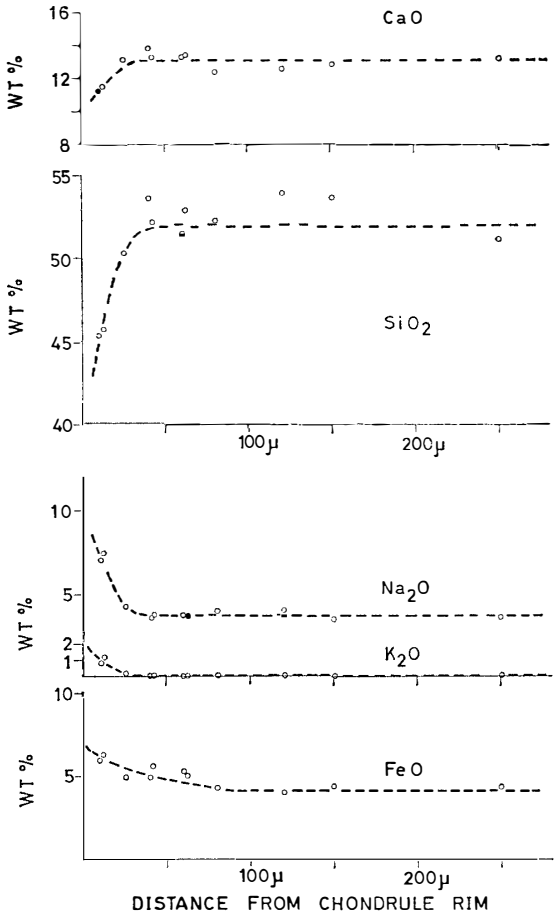

Fig. 12. Chemical zoning of the clean groundmass glass and the peripheral dark glass in No. 1 chondrule.

5.4. No. 12 chondrule (IP type)

This chondrule is holocrystalline and about 800 microns in diameter. It consists of densely packed olivine grains and interstitial pyroxene, plagioclase and nepheline. Their chemical compositions are tabulated in Tables 9 and 10. Olivines show remarkable chemical zonation of Mg/(Mg+Fe) mole ratios from 0.97 to 0.67. Low-Ca clinopyroxenes show polysynthetic twinning and occur in the peripheral part of this chondrule. Plagioclases associate intimately with pigeonitic pyroxenes. Small nepheline grains always occur in contact with plagioclase grains. Crystallization sequence of pyroxenes is schematically represented by the solidus curve of B in Fig. 11.

5.5. No. 23 chondrule (mSP type)

This chondrule is about 500 microns in diameter and consists of olivine, pyroxene and interstitial clean glass. Their chemical compositions are tabulated in Tables 10 and 11. Olivine grains are euhedral to subhedral and zone from 0.96 to 0.78 in Mg/(Mg+Fe) ratios, whereas pyroxenes are fairly magnesian. Orthopyroxenes and

low-Ca clinopyroxenes showing polysynthetic twinning occur in the peripheral part of this chondrule, but high-Ca clinopyroxenes occur in the central part. The crystallization of pyroxenes is represented by D in Fig. 11.

5.6. No. 36 chondrule (fSP type)

This chondrule is about 500 microns in diameter and consists of euhedral olivine crystals and black devitrified glass. The olivines are fairly homogeneous at Mg/(Mg+Fe)=about 0.65. The chemical composition of the black devitrified groundmass glass is tabulated in Table 11, and is represented by a normative composition of ferrous olivine+high-Ca pyroxene+albite+nepheline, lacking in the normative orthopyroxene component. The crystallizing phase was only olivines, and the residual liquid was quenched as groundmass glass.

6. Formation of Fine-grained CAI's and AOI's

In general, fine-grained CAI's and AOI's contain not only the components of high-temperature condensates of the solar nebula, but also variable amounts of low-temperature components such as alkalis and FeO (McSween, 1977c). This fact is an important point for origin of these inclusions and makes the formation theory complex. The theories on origin of these inclusions are summarized as follows: (1) Direct condensation from vaporized gas (Martin and Mason, 1974). (2) Condensation in a mixing zone between supernova remnants and the solar cloud (Wark, 1979). (3) Various degrees of mixing of the two components, residual droplets and recondensed fine-grained materials (Kornacki, 1981). (4) Devitrification of direct-condensed liquid droplets except some fine-grained CAI's formed by the aggregation of distillation residues (Cohen, 1981). (5) Residues of throughly reacted CAI's by metamorphism or aqueous reaction on a planetary body (Armstrong *et al.*, 1982).

Another important point on origin of fine-grained CAI's is that typical fine-grained CAI's (type F aggregates of Wark (1979)) consist of spinel-rich nodules and debris, the nodules showing a rim structure similar to that of many coarse-grained CAI's (Wark, 1979). These rims around the nodules include nepheline and FeO-bearing minerals (Wark and Lovering, 1977). Thus the introduction of alkalis and FeO into fine-grained CAI's may be due to a similar process to the formation of the rim structure around coarse-grained CAI's. According to MacPherson *et al.* (1981), the rim layering around coarse-grained CAI's in Allende were formed at a constant temperature by the introduction of Si, Na and Fe from the surrounding nebula gas and the release of excess Ca and Al. Therefore, the theory on origin of fine-grained CAI's must include gas reactions between high-temperature condensates and the surrounding gas.

6.1. Some fine to medium-grained CAI's in ALH-77003 show a rim structure around them. Two fine to medium-grained inclusions Nos. 43 (Fig. 7e) and 200 consist of spinel, fassaitic pyroxene, and fine-grained black materials, the rims showing double structure of outer pyroxene rim and inner black rim. The inner black rims occur between the outer pyroxene rim and central medium-grained part consisting of spinel and fassaitic pyroxene as shown in Fig. 13b. The outer pyroxene rims are aluminous

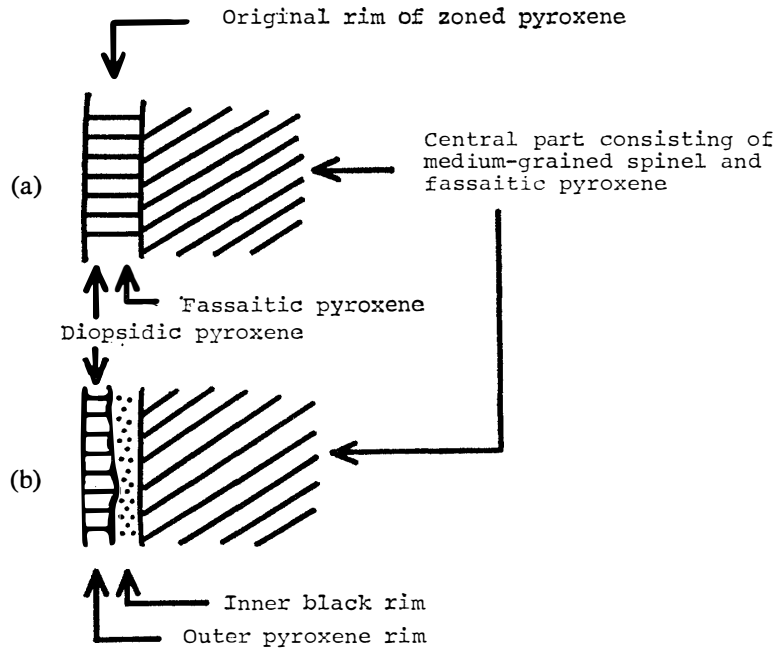

Fig. 13. Schematic figures of rim structure of some fine to medium-grained CAI's. (a): Original structure of the rim. (b): Present structure of the rim after the reactions with the surrounding gas.

Table 12. Chemical compositions of the inner black rims of fine to medium-grained CAI's of Nos. 43′ and 200. (1) and (2) are the chemical compositions of the products of reaction equations (1) and (2), respectively (see text).

	43′–A1 Black rim	43′–A2 Black rim	200–A Black rim	200–D Black rim	(1)	(2)
Na_2O	12.28	10.58	8.39	7.02	14.0	9.7
MgO	4.36	4.67	5.56	6.52	4.5	6.3
Al_2O_3	41.84	41.46	36.45	39.88	46.2	40.0
SiO_2	26.74	26.11	26.05	23.27	27.1	28.3
K_2O	1.37	1.27	1.50	1.06		
CaO	1.83	2.35	4.68	4.57	0.0	4.4
TiO_2		0.45	0.64	2.02		
Cr_2O_3	0.07	0.08	0.08	0.10		
MnO	0.05					
FeO	8.95	9.78	10.58	14.06	8.1	11.3
Total	97.48	96.74	93.92	98.49	100.0	100.0

diopsidic pyroxenes whereas the inner black rims are very fine-grained materials rich in alkalis and FeO. The chemical compositions of the inner black rims are tabulated in Table 12. The inner black rims are thought to be formed after the formation of the outer pyroxene rims, and the model for origin of the inner black rims is schematically shown in Fig. 13. Originally, pyroxene rims are considered to be broader, consisting of zoned magnesian pyroxenes from inner fassaitic pyroxene to outer diopsidic pyroxene. When the surrounding gas became rich in alkalis and FeO components,

the inner fassaitic pyroxenes reacted with the surrounding gas to form the inner black rims. The possible reactions to produce the inner black rims from fassaitic pyroxenes are as follows,

$$\underset{\text{Fas}}{6Ca_2MgAlSi_3AlO_{12}} + \underset{\text{Gas}}{6Na} + \underset{\text{Gas or Met}}{1.5Fe} + \underset{\text{Gas}}{24H_2} \rightarrow \underset{\text{Ne}}{6NaAlSiO_4} + \underset{\text{Sp}}{3(Mg_{0.5}Fe_{0.5})Al_2O_4} + \underset{\text{Gas}}{12Ca} + \underset{\text{Gas}}{4.5Mg} + \underset{\text{Gas}}{12SiO} + \underset{\text{Gas}}{24H_2O}, \quad (1)$$

$$\underset{\text{Fas}}{5Ca_2MgAlSi_3AlO_{12}} + \underset{\text{Gas}}{4Na} + \underset{\text{Gas or Met}}{2Fe} + \underset{\text{Sp}}{17H_2} \rightarrow \underset{\text{Ne}}{4NaAlSiO_4} + \underset{\text{Px}}{Ca(Mg_{0.5}Fe_{0.5})Si_2O_6} + \underset{\text{Sp}}{3(Mg_{0.5}Fe_{0.5})Al_2O_4} + \underset{\text{Gas}}{9Ca} + \underset{\text{Gas}}{3Mg} + \underset{\text{Gas}}{9SiO} + \underset{\text{Gas}}{17H_2O}, \quad (2)$$

where Fas, Met, Ne, Sp and Px are fassaite, metal, nepheline, spinel and pyroxene, respectively. Equation (1) can produce black rims rich in alkalis and Al_2O_3 and poor in CaO, the products being similar to the inner black rim of No. 43′ (Table 12). Equation (2) gives the reaction products of nepheline, high-Ca pyroxene and spinel, resulting in CaO-bearing products similar to the rim of No. 200 inclusion. The bluk chemical compositions of these product assemblages by the eqs. (1) and (2) are calculated and tabulated in Table 12. The calculated chemical compositions well coincide with the compositional range of the inner black rims of Nos. 43′ and 200 inclusions.

However, the release of the excess Ca, Mg and SiO into low-temperature solar nebular gas is difficult because these components are main high-temperature condensates and can not dissolve in the low-temperature nebula gas. Two possibilities for this difficulty are considered. One is that the surrounding gas had a chemical composition different from the solar abundances and extremely depleted in Ca, Mg and SiO. The other is that the released Ca, Mg and SiO species precipitated elsewhere as silicates or other minerals with other components of the surrounding nebula gas. In this case the gas species of the right hand sides of eqs. (1) and (2) are presented for the porpose of symplification. The latter possibility was chosen by MACPHERSON *et al.* (1981), but it is unknown whether the latter possibility is more reasonable than the former possibility or not. As already stated in the foregoing sections, some chondrules in ALH-77003 show a remarkable zoning of chemical compositions in their peripheral groundmass glass. This chemical zoning is considered to be formed by the addition of alkalis and FeO components to the peripheral groundmass glass and the release of SiO_2 and CaO components from the chondrules. This supports the reality of the release of Ca and SiO species of eqs. (1) and (2) from the fine to medium-grained CAI's.

The central parts of the inclusions Nos. 43′ and 200 consist mainly of ferrous spinel with minor amounts of fassaitic pyroxene. The fassaitic pyroxenes may not have suffered the gas reactions because they were included completely by the spinel crystals.

But the ferrous spinels may have been produced from magnesian spinels by the following equation;

$$\underset{\text{Sp}}{MgAl_2O_4} + \underset{\text{Gas or Met}}{Fe} \rightarrow \underset{\text{Sp}}{FeAl_2O_4} + \underset{\text{Gas}}{Mg}. \quad (3)$$

This equation is an exchange reaction of Mg and Fe between spinels and the surround-

ing gas, and magnesian spinels of the inclusions can become ferrous through reaction (3), their mole ratios of MgO/(MgO+FeO) resulting in about 0.5, as shown in Table 8.

In ALH-77003, many fine-grained CAI's consist of black aggregates of fine-grained materials similar to the inner black rims of Nos. 43′ and 200 inclusions. Thus if they were formed by the reactions (1) and (2), we can estimate the original compositions by reversing the reaction equations. From eqs. (1) and (2), it is considered that the CaO and SiO_2 in fine-grained CAI's are expelled by the nearly twice number of $NaO_{0.5}$ molecules. In Fig. 14, the chemical compositions of fine-grained CAI's are plotted in (Ca+2Na)-Al-(Si+2Na) diagram. The fine-grained CAI's are plotted along the tie line of spinel and fassaitic pyroxene, and the most of them coincide with the chemical composition of fassaitic pyroxene. This plotting indicates that the original materials of fine-grained CAI's in ALH-77003 consist mainly of fassaitic pyroxene with variable amounts of spinel. In Fig. 14 type-B CAI's (GROSSMAN, 1975) are shown together for reference, which are composed mainly of fassaitic pyroxene and spinel. The original materials of some fine-grained CAI's well coincide with the compositions of type-B CAI's, indicating that some fine-grained CAI's may have derived from the type-B CAI's by the reactions of eqs. (1) and (2).

6.2. AOI's in ALH-77003 are also plotted in Fig. 14. They locate nearly along the solar condensate trend of high-temperature range. However, they include abundant amounts of FeO with minor alkali contents. The minor contents of alkalis may be introduced by the reactions of eqs. (1) and (2), but the large contents of FeO can not be explained by eqs. (1), (2) and (3) because fassaitic pyroxene and spinel are minor constituents in these AOI's. There are two possibilities for the introduction of FeO into AOI's. First idea is that the ferrous olivines of AOI's condensed directly from the nebula gas of high FeO activity. Secondly, the FeO contents of AOI's were introduced by a gas reaction after the condensation of primary magnesian olivines and the formation of magnesian AOI's. A possible reaction is;

$$\underset{\text{Ol}}{Mg_2SiO_4} + 2Fe \rightarrow \underset{\text{Ol}}{Fe_2SiO_4} + 2\underset{\text{Gas}}{Mg}. \qquad (4)$$

This equation is an exchange reaction of Mg and Fe between the olivines of AOI's and the surrounding gas, and can introduce large amounts of FeO into the AOI's in the condition similar to that of eqs. (1), (2) and (3).

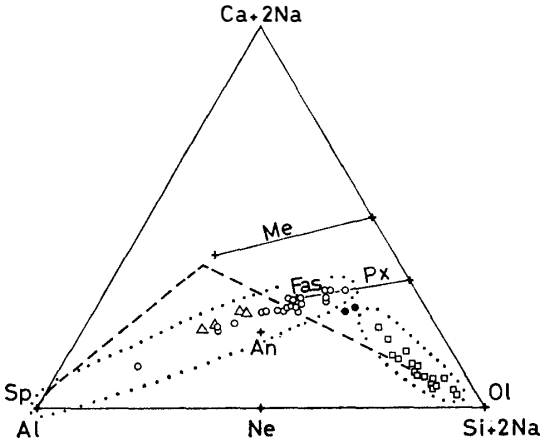

Fig. 14. Atomic plotting of (Ca+2Na)-Al-(Si+2Na) for fine to medium-grained CAI's (open circle), AOI's (open square), and the intermediate type inclusions (solid circle) in ALH-77003. For reference, type-B CAI's (open triangle, quoted from GROSSMAN, 1975) are plotted together. Dashed line is the solar condensate trend. Abbreviations of Me, Fas, Px, Ol, An, Ne and Sp are melilite solid solution, fassaite, high-Ca pyroxene solid solution, olivine, anorthite, nepheline and spinel, respectively.

6.3. Two inclusions (Nos. 71–1 and 105 in Table 1) are fine-grained aggregates including abundant fine olivine grains and are intermediate in texture between fine-grained CAI's and AOI's. These intermediate inclusions are plotted between the fine-grained CAI's and AOI's in Fig. 14. The original materials of these intermediate type are considered to be a mixture of fassaitic pyroxene and olivine, and the fassaites reacted with the surrounding gas by reactions (1) and (2) to be fine-grained aggregates containing alkalis and FeO. The existence of the intermediate type indicates that the original materials of fine-grained CAI's and AOI's had an intimate genetical relation prior to reactions (1) to (4).

6.4. In conclusion, the original materials of fine-grained CAI's in ALH-77003 were composed mainly of fassaitic pyroxenes with variable amounts of spinels, some inclusions having thin zoned rims of fassaitic to diopsidic pyroxenes around them. The original materials of AOI's consisted mainly of olivines with minor fassaitic pyroxenes. When the activities of Na_2O and FeO components in the surrounding gas became high, the reactions of (1), (2), (3) and (4) took place. The fassaitic pyroxenes changed to fine-grained aggregates including alkalis and FeO, and spinels and probably olivines may have become ferrous, resulting in fine-grained CAI's and AOI's prior to the accretion onto the parental body of ALH-77003. Some chondrules were brought into the similar atmosphere and suffered the addition of alkalis and FeO and the release of SiO_2 and CaO, resulting in zoned chondrules.

7. Chondrules, Devitrified Glass Fragments and Matrix

The fine-grained CAI's and AOI's in ALH-77003 are considered to change their chemical compositions by reactions (1) to (4), and their compositions deviate more or less from the solar condensate trend. However, the other constituent units, mIP, mSP and fSP chondrules, devitrified glass fragments, and the matrix coincide well with the solar condensate trend except for minor modifications. The average chemical compositions of each type of chondrules, devitrified glass fragments, and the matrix are tabulated in Table 13 with reference to the solar abundances (CAMERON, 1973) and the matrix of the Allende meteorite (IKEDA, in preparation).

7.1. Matrix, devitrified glass fragments and fSP chondrules

The matrix, devitrified glass fragments, and fSP chondrules show similar chemical compositions (Table 13), and they are considered to have cogenetic relationship. The matrix of ALH-77003 is very similar in chemical composition to that of the Allende meteorite except that the CaO content of the former is extremely depleted in comparison with the latter. The chemical compositions of the devitrified glass fragments nearly coincide with the solar abundances. The chemical compositions of fSP chondrules are decidedly different from those of the mIP and mSP chondrules, and rather resemble those of the devitrified glass fragments, except that the fSP shows higher CaO content than the devitrified glass fragments.

The chemical compositions of the fSP type include small amounts of orthopyroxene normative component whereas those of the matrix are free from this component, the devitrified glass fragments being intermediate. In addition, the fSP, the devitrified

Table 13. Average chemical compositions of mIP, mSP and fSP chondrules, devitrified glass fragments, and matrix in ALH-77003. MA and SA are the average composition of the matrix in the Allende meteorite and the solar abundances, respectively. The average composition of the devitrified glass fragments is calculated from Table 6 except for the No. 32.5 fragment which is considered to be a fragment of groundmass glass of fSP chondrules. The compositions of the matrices and the solar abundance are normalized to the total of 100 wt%.

	mIP	mSP	fSP	glass-fragment	matrix	MA	SA
Na_2O	0.60	1.60	1.00	1.02	0.29	0.37	1.05
MgO	33.48	28.47	22.62	25.30	26.88	22.98	24.74
Al_2O_3	3.64	3.28	2.04	2.08	2.35	3.04	2.51
SiO_2	47.87	52.63	40.06	37.00	33.33	33.94	34.81
CaO	3.68	4.25	3.63	2.04	0.46	3.06	2.34
FeO	9.18	8.27	28.83	30.13	36.68	36.61	34.54
Total	98.45	98.50	98.18	97.57	100.00	100.00	100.00

glass fragments and the matrix are high in FeO, and the amounts of FeO increase from the fSP to the matrix. These features may be due to the following equation;

$$\underset{\text{Px}}{MgSiO_3} + \underset{\text{Gas or Met}}{Fe} + \underset{\text{Gas}}{H_2O} \rightarrow \underset{\text{Ol}}{MgFeSiO_4} + \underset{\text{Gas}}{H_2}. \quad (5)$$

The original materials of fSP chondrules and the matrix may correspond to the condensates during the last stage of and after the reaction (5), respectively. Equation (5) means the silicate condensates of low temperature range must show MgO/(MgO+FeO) mole ratios of about 0.5, coinciding with the fact that the average ratios of the matrix is about 0.57 (Table 13).

The chemical compositions of the matrix include the normative nepheline component although the fSP chondrules are free from this component. This may be due to the reaction:

$$\underset{\text{Ab}}{NaSi_3AlO_8} + 4\underset{\text{Gas or Met}}{Fe} + 4\underset{\text{Gas}}{H_2O} \rightarrow \underset{\text{Ne}}{NaSiAlO_4} + 2\underset{\text{Ol}}{Fe_2SiO_4} + 4\underset{\text{Gas}}{H_2}, \quad (6)$$

where Ab and Ne are albite and nepheline, respectively. This equation introduces the normative nepheline component and also the FeO component into low temperature condensates, but the amounts of FeO introduced by this equation are small in comparison with those by eq. (5) because the pyroxenes are a major phase and overwhelm the albite amount in the solar condensates prior to reactions (5) and (6). Reaction (6) may take place at the temperatures lower than reaction (5), because nepheline can not stably coexist with low-Ca pyroxene.

In conclusion, the fSP chondrules are considered to be formed from the materials which condensed during reaction (5) and prior to reaction (6). The materials which were formed at intermediate temperatures between fSP and matrix became the devitrified glass fragments by melting and subsequent fragmentation and devitrification. The dust which were formed at the lowest temperatures after the reactions (5) and (6) became the matrix at the accretion onto the parent body of ALH-77003. The low contents of CaO and Na_2O in the matrix may be due to the fractionation and separa-

tion of high-Ca pyroxenes and nephelines or albites prior to or during the formation of dusts in the solar nebula, whereas the original materials of the devitrified glass fragments contain both minerals in the same amounts as the low-temperature solar condensates.

7.2. The mIP and mSP chondrules

The chemical compositions of mIP and mSP chondrules are similar except for the Na_2O, MgO and SiO_2 contents. The mIP is poorer in Na_2O and SiO_2 and richer in MgO. This means that the mIP contains larger amounts of normative olivine than the mSP, whereas the latter contains larger amounts of normative orthopyroxene and albite. According to the condensation theory of GROSSMAN and LARIMER (1974), the condensation of calcic plagioclase begins at 1362 K at total pressure of 10^{-3} atm, and enstatite begins to condensate at about 1350 K, consuming forsterite. Below 1100 K, enstatite exceeds forsterite in the silicate condensates, and at the same time plagioclase becomes sodic. This change of condensing phases corresponds to the solar trend from f to g in Figs. 2, 3 and 4. The average chemical composition of mIP corresponds to silicate condensates at temperatures higher than about 1100 K, and the average composition of mSP corresponds to temperatures lower than about 1100 K. However, these high temperature condensates should be free from FeO, although the mIP and mSP contain considerable amounts of FeO. Moreover, the mIP contains some Na_2O. Therefore, the high-temperature condensates must be contaminated by the lower temperature condensates, such as FeO and alkalis, prior to or during the melting events which formed silicate melt droplets resulting finally in chondrules.

The mIP and mSP chondrules include variable amounts of opaque minerals such as kamacite, taenite and/or troilite. However, the amounts of these minerals are small for most chondrules, and the bulk compositions of these chondrules never plot along the metal-bearing condensate trend. Therefore, the metal condensates must have fractionated or separated from the silicate and oxide condensates prior to the formation of chondrules. It is considered that the separated metal condensates formed the core of primitive planetesimals whose mantles consisted of the solar condensates of silicates and oxides with small amounts of opaque minerals. When these planetesimals collided with each other, silicate melt droplets may have formed from the mantle materials of the primitive planetesimals (KIFFER, 1975), and some materials in the cores may have fragmented to form the opaque mineral fragments commonly observed in ALH-77003.

The genetical relationship of the mIP and mSP chondrules with the fSP, devitrified glass fragments, and matrix is unknown, but it is possible that the original materials of the former two were formed mainly prior to or during the initial stage of reaction (5) and those of the latter three were produced mainly during the last stage of or after the reaction.

8. Conclusions

Conclusions of this paper are summarized as follows.

1) Fine-grained CAI's in ALH-77003 were originally materials consisting mainly of fassaitic pyroxenes with variable amounts of spinels. They changed their chemical

compositions by reactions with the surrounding gas at low temperatures, and became rich in alkalis and FeO.

2) AOI's are considered to have a cogenetic relation with fine-grained CAI's. The alkali contents in AOI's were introduced from the surrounding gas by the same reactions as those in fine-grained CAI's.

3) The mIP and mSP chondrules were formed mainly from the high-temperature condensates of the solar nebula after the separation of metallic condensates. The condensation temperature for the mIP and mSP chondrules are higher and lower than 1100 K, respectively, at total gas pressure of 10^{-3} atm.

4) Some chondrules were brought into a gas rich in alkalis and FeO components and suffered the addition of alkalis and FeO and the release of SiO_2 and CaO, resulting in zoned chondrules.

5) The matrix and the original materials of fSP and devitrified glass fragments were made up mainly from low-temperature condensates of the solar nebula. The condensation temperatures of the former were slightly lower than the latters. The fractionation of high-Ca pyroxenes, nephelines and/or albites took place in the solar nebula, and these minerals were depleted in the matrix of ALH-77003.

Acknowledgments

The author thanks Prof. N. ONUMA for discussion and Prof. M. KUBOTA for permitting the use of the electron-probe microanalyzer.

References

ALLEN, J. M., GROSSMAN, L., LEE, L. and WASSERBURG, G. J. (1980): Mineralogy and petrography of HAL, an isotopically-unusual Allende inclusion. Geochim. Cosmochim. Acta, **44**, 685–699.

ARMSTRONG, J. T. and WASSERBURG, G. J. (1981): The Allende pink angel: Its mineralogy, petrology, and the constraints of its genesis. Lunar and Planetary Science XII. Houston, Lunar Planet. Inst., 25–27.

ARMSTRONG, J. T., MEEKER, G. P., HUNEKE, J. C. and WASSERBURG, G. J. (1982): The blue angel: I. The mineralogy and petrogenesis of a hibonite inclusion from the Murchison meteorite. Geochim. Cosmochim. Acta, **46**, 575–595.

BENCE, A. E. and ALBEE, A. L. (1968): Empirical correction factors for the electron microanalysis of silicates and oxides. J. Geol., **76**, 382–403.

BOYD, F. R. and SCHAIRER, J. F. (1964): The system $MgSiO_3$-$CaMgSi_2O_6$. J. Petrol., **5**, 275–309.

BUNCH, T. E. and CHANG, S. (1980): Carbonaceous chondrites-II. Carbonaceous chondritic phyllosilicates and light elements geochemistry as indications of parental body processes and surface conditions. Geochim. Cosmochim. Acta, **44**, 1543–1577.

CAMERON, A. G. W. (1973): Abundances of the elements in the solar system. Space Sci. Rev., **15**, 121–146.

COHEN, R. (1981): A study of the Mokoia C3(V) carbonaceous chondrite and the origin of CAI's. Lunar and Planetary Science XII. Houston, Lunar Planet. Inst., 163–165.

GREEN II, H. W., RADCLIFFE, S. V. and HEUER, A. H. (1971): Allende meteorite: A high-voltage electron petrographic study. Science, **172**, 936–939.

GROSSMAN, L. (1975): Petrography and mineral chemistry of Ca-rich inclusions in the Allende meteorite. Geochim. Cosmochim. Acta, **39**, 433–454.

GROSSMAN, L. and LARIMER, J. W. (1974): Early chemical history of the solar system. Rev. Geophys.

Space Phys., **12**, 71–101.

IKEDA, Y. (1980): Petrology of ALH-764 chondrite (LL3). Mem. Natl Inst. Polar Res., Spec. Issue, **17**, 50–82.

IKEDA, Y., KIMURA, M., MORI, H. and TAKEDA, H. (1981): Chemical compositions of matrices of unequilibrated ordinary chondrites. Mem. Natl Inst. Polar Res., Spec. Issue, **20**, 124–144.

KALLEMEYN, G. W. and WASSON, J. T. (1981): The compositional classification of chondrites-I. The carbonaceous chondrite groups. Geochim. Cosmochim. Acta, **45**, 1217–1230.

KIEFFER, S. W. (1975): Droplet chondrules. Science, **189**, 333–340.

KORNACKI, A. S. (1981): Are CAI's condensates or distillation residues? Evidence from a comprehensive survey of fine- to medium-grained inclusions in the Allende C3(V) carbonaceous chondrite. Lunar and Planetary Science XII. Houston, Lunar Planet. Inst., 562–564.

LEVIN, E. M., ROBBINS, C. R. and MCMURDIE, H. F. (1964): Phase Diagrams for Ceramists. Ed. and Pub. by Am. Ceram. Soc.

MACPHERSON, G. J., GROSSMAN, L., ALLEN, J. M. and BECKETT, J. R. (1981): Origin of rims on coarse-grained inclusions in the Allende meteorite. Proc. Lunar Planet. Sci. 12B, 1079–1091.

MARTIN, P. M. and MASON, B. (1974): Major and trace elements in the Allende meteorite. Nature, **249**, 333–334.

MARVIN, U. and MASON, B. (1980): Catalog of Antarctic meteorite, 1977–1978. Smithson. Contrib. Earth Sci., **23**, 50 p.

MCSWEEN, H. Y., Jr. (1977a): On the nature and origin of isolated olivine grains in carbonaceous chondrites. Geochim. Cosmochim. Acta, **41**, 411–418.

MCSWEEN, H. Y., Jr. (1977b): Carbonaceous chondrites of the Ornans type: A metamorphic sequence. Geochim. Cosmochim. Acta, **41**, 477–491.

MCSWEEN, H. Y., Jr. (1977c): Petrographic variations among carbonaceous chondrites of the Vigarano type. Geochim. Cosmochim. Acta, **41**, 1777–1790.

MCSWEEN, H. Y., Jr. (1977d): Chemical and petrographic constraints on the origin of chondrules and inclusions in carbonaceous chondrites. Geochim. Cosmochim. Acta, **41**, 1843–1860.

MCSWEEN, H. Y., Jr. and RICHARDSON, S. M. (1977): The composition of carbonaceous chondritic matrix. Geochim. Cosmochim. Acta, **41**, 1145–1161.

OSBORN, T. W., WARREN, R. G., SMITH, R. H., WAKITA, H., ZELLMER, D. L. and SCHMITT, R. A. (1974): Elemental composition of indivisual chondrules from carbonaceous chondrites, including Allende. Geochim. Cosmochim. Acta, **38**, 1359–1378.

VAN SCHMUS, W. R. and HAYES, J. M. (1974): Chemical and petrographic correlations among carbonaceous chondrites. Geochim. Cosmochim. Acta, **38**, 47–64.

WARK, D. A. (1978): Early solar system stratigraphy: The condensation sequence from Allende to chondrites, and the origin of chondrites. Lunar and Planetary Science IX. Houston, Lunar Planet. Inst., 1208–1210.

WARK, D. A. (1979): Birth of the presolar nebula: The sequence of condensation revealed in the Allende meteorite. Astrophys. Space Sci., **65**, 275–295.

WARK, D. A. and LOVERING, J. F. (1977): Marker events in the early evolution of the solar system: Evidence from rims in Ca-Al-rich inclusions in carbonaceous chondrites. Proc. Lunar Sci. Conf. 8th, 95–112.

WARK, D. A. and LOVERING, J. F. (1978): Classification of Allende coarse-grained Ca-Al-rich inclusions. Lunar and Planetary Science IX. Houston, Lunar Planet. Inst., 1211–1213.

WASSON, J. T. (1974): Meteorites. Berlin, Springer, 316 p. (Mineral and Rocks, Vol. 10).

(*Received May 19, 1982; Revised manuscript received October 25, 1982*)